Atmospheric Rivers and Weather Types in Aotearoa New Zealand: a two-way story

Benjamin Pohl[1]*; Hamish D. Prince[2]; Jonathan Wille[3]; Daniel G. Kingston[4]; Nicolas J. Cullen[4]; Nicolas Fauchereau[5]

[1] Biogéosciences, UMR6282 CNRS / Université de Bourgogne Franche-Comté, Dijon, France
[2] Department of Atmospheric and Oceanic Sciences, University of Wisconsin-Madison, Madison, WI, USA
[3] Université Grenoble Alpes/CNRS/IRD/G-INP, IGE, Grenoble, France
[4] School of Geography, University of Otago, Dunedin, New Zealand
[5] National Institute of Water and Atmospheric Research, Auckland, New Zealand

Submitted to
JGR: Atmospheres
30 May 2022

Keypoints

- Weather types are major drivers of atmospheric rivers (frequency, angle, moisture transport direction and landfalling region)
- Atmospheric rivers explain part of within-type diversity (circulation and rainfall anomalies)
- Combined or separate effects of weather types and atmospheric rivers strongly vary from one region of Aotearoa New Zealand to another

*** Corresponding Author Address**
Benjamin Pohl — Laboratoire Biogéosciences
6 boulevard Gabriel — 21000 Dijon — France
benjamin.pohl@u-bourgogne.fr / (+33) 3 80 39 38 21

Abstract

Here, we analyze the inter-relationships between weather types (WTs) and atmospheric rivers (ARs) around Aotearoa New Zealand (ANZ), their respective properties, as well as their combined and separate influence on daily precipitation amounts and extremes. Results show that ARs are often associated with 3-4 WTs, but these WTs change depending on the regions where ARs landfall. The WTs most frequently associated with ARs generally correspond to those favoring anomalously strong westerly wind in the mid-latitudes, especially for southern regions of ANZ, or northwesterly anomalies favoring moisture export from the lower latitudes, especially for the northern regions.

WTs and ARs show strong within-type and inter-event diversity. The synoptic patterns of the WTs significantly differ when they are associated with AR occurrences, with atmospheric centers of actions being shifted so that moisture fluxes towards ANZ are enhanced. Symmetrically, the location, angle, and persistence of ARs appear strongly driven by the synoptic configurations of the WTs. Although total moisture transport shows weaker WT-dependency, it appears strongly related to zonal wind speed to the south of ANZ, or the moisture content of the air mass to the north. Finally, WT influence on daily precipitation may completely change depending on their association, or lack thereof, with AR events. WTs traditionally considered as favorable to wet conditions may conceal daily precipitation extremes occurring during AR days, and anomalously dry days or near-climatological conditions during non-AR days.

Key-Words

Atmospheric rivers — weather types — Aotearoa New Zealand — atmospheric centers of action — vapor transport — synoptic-scale variability

1. Introduction

Atmospheric rivers (ARs) have been receiving increasing attention from the scientific community [*Ralph et al.*, 2017]. According to the Glossary of Meteorology, they consist in "long, narrow, and transient corridor[s] of strong horizontal water vapor transport that is typically associated with a low-level jet stream ahead of the cold front of an extratropical cyclone" [*Ralph et al.*, 2018]. AR genesis occurs more frequently over oceans [*Zhu and Newell*, 1994; *Guan and Waliser*, 2019], and ARs are a major conveyor belt of moisture towards the continent and land masses [ibid.]. When they reach land, they can bring heavy precipitation: this is especially the case when and where such ARs encounter a land mass with marked topography, which forces the strong moisture flux to ascend.

Because of its insularity (Fig. 1a) and sharp topography almost perpendicular to the dominant westerly winds at latitudes where oceans largely prevail, Aotearoa New Zealand (ANZ) is recurrently affected by AR events [*Prince et al.*, 2021a]. AR events landfalling in ANZ have been identified as the key drivers for a vast majority of daily rainfall extremes [*Reid et al.*, 2021; *Shu et al.*, 2021], floods [*Kingston et al.*, 2016], and extreme ablation and snowfall [*Porhemmat et al.*, 2021a, 2021b] impacting the mountain glaciers [*Little et al.*, 2019]. These extreme flooding events can cause instability in agriculture and hydroelectric power sectors [*Dravitzki and McGregor*, 2011] while inflicting long-term social harm in rural regions of ANZ [*Smith et al.*, 2011]. With ARs projected to become more frequent and transport more moisture towards ANZ under climate change [*Espinoza et al.*, 2018], it is crucial to understand the circulation patterns that influence their behavior.

Looking at the synoptic-scale dynamics, the AR life cycle often begins where Rossby wave breaking in the exit regions of mid-latitude jets streams initiates the penetration of troughs into the subtropics, creating a channel for poleward moisture transport [*Hoskins et al.*, 1985]. This enhanced poleward transport of heat and moisture increases upper-level latent heat release encouraging vertical motion from increased diabatic heating, which creates downstream negative potential vorticity anomalies [*Pfahl et al.*, 2015]. The injection of negative potential vorticity air masses into higher latitudes fuels atmospheric blocking which allows ARs to persist through multiple extratropical cyclone life cycles [*Sodemann and Stohl*, 2013], while aiding in explosive cyclone deepening [*Zhu and Newell*, 1994]. Therefore, ARs are not necessarily attached to extratropical cyclones, but the two are mutually beneficial to their development and transport [*Zhang et al.*, 2019].

Because they are embedded in the synoptic-scale variability, but also contribute to shape it in return, ARs tend to show preferential associations, and increased probability, when co-occurring with favorable weather patterns [*Kingston et al.*, 2022]. Around ANZ, a set of 12 weather types (WTs) based on a clustering of 1000hPa geopotential height fields has been developed by Kidson [2000: K2K hereafter] to account for the space-time variability of such synoptic weather patterns. These WTs have been extensively used by the regional climate community, for paleoclimate reconstructions in the Holocene [*Lorrey et al.*, 2007, 2008, 2012; *Ackerley et al.*, 2011] and Little Ice Age [*Lorrey et al.*, 2014], and to analyze climate change projections [*Parsons et al.*, 2014]. Significant relationships have been established between these WTs and the Madden–Julian oscillation [*Fauchereau et al.*, 2016], the interdecadal Pacific oscillation [*Lorrey et al.*, 2007], and the Southern Hemisphere large-scale background conditions [*Renwick*, 2011]. At the more local and regional scales, these WTs have been shown to drive daily climate anomalies [K2K; *Renwick*, 2011], seasonal rainfall anomalies [*Lorrey et al.*, 2007], and to modulate ocean wave heights [*Coggins et al.*, 2016] and ocean–atmosphere coupled summer heatwaves [*Salinger et al.*, 2020]. Recently, they have been shown to conceal strong within-type variability [*Pohl et al.*, 2021a: P21 hereafter], a given type being associated with atmospheric ridges and troughs highly variable in intensities and locations. These within-type changes are partly driven by large-scale climate conditions, and explain about the same fraction of regional variability as changes in WT occurrence.

Although evidence has been provided [*Kingston et al.*, 2022] that AR occurrence is significantly modified by the 12 WTs of K2K, several questions remain unresolved to date, including (but not restricted to) the following points:

— How WTs influence AR properties (vertically integrated vertical vapor transport [IVT], main direction / angle of the ARs, persistence, total vapor transport integrated over the whole life cycle of the AR). These descriptors may determine the moisture sources of the ARs, and are very likely to be modulated by the synoptic configurations, as shown e.g. by *Pohl et al.* [2021b] further south for ARs developing over the Southern Ocean and landfalling in East Antarctica.

— WT patterns may differ when they co-occur vs. when they do not co-occur with AR events. Part of the strong within-type diversity linked to changes in the location and intensities of atmospheric centers of action (ACAs: P21) could partly relate to the development (or lack thereof) of ARs in the ANZ sector.

— Although WT influence has been extensively assessed [K2K; *Lorrey et al.*, 2007; *Renwick*, 2011], their separate and combined influence with ARs on daily precipitation amounts, including extremes, remains to be determined. The picture of precipitation changes from one WT to another could be strongly modified depending on their co-occurrence (or lack thereof) with ARs.

— Finally, it seems important to assess how these results change from one region of ANZ to another, depending on the latitude, terrain exposure, local climate, coastline / land-sea contrasts and topography. This is expected to be particularly interesting for ANZ considering previously documented substantial regional differences in AR occurrence and characteristics [*Prince et al.*, 2021a; *Kingston et al.*, 2022] and unusual situation of landfalling ARs occurring on both windward and leeward coasts relative to the prevailing large-scale circulation.

This paper aims at filling these gaps, and proposes therefore to analyze the inter-connections between ARs, WTs and precipitation amounts across ANZ. Both ARs and WTs are considered not only in terms of (co-)occurrence, but also through their properties, as inferred by the set of descriptors respectively proposed by Guan and Waliser [2019] and P21. Daily precipitation fields are derived from a 5-km resolution interpolated product constrained by observational networks, that allows for a detailed analysis of terrain influence on the spatial distribution of daily amounts.

In the following, Section 2 presents the data and methods used in this work. Section 3 presents the AR count in each region of ANZ, and their association with WTs. Section 4 next focuses on their separate vs. combined influences on daily precipitation, considering both anomalies and daily extremes. Section 5 addressed the co-occurrence of ARs and WTs, how they change from one part of ANZ to another, and assesses to which extent their intrinsic properties are interdependent. Finally, Section 6 summarizes and discusses our main results.

2. Data and Methods

2.1 Data

Atmospheric fields used here are taken from the ERA5 ensemble reanalysis [*Hersbach et al.*, 2020]. ERA5 is the fifth generation of atmospheric reanalysis released by the European Centre for Medium-Range Weather Forecasts. It currently covers the period 1979 onward (with an extension to 1950 but with weaker constraint by assimilation due to the lack of satellite data) and includes a 10-member ensemble to quantify uncertainties associated with the density and quality of the assimilated data. In this work, we use both the regular 0.25° x 0.25° and 0.5° x 0.5°grids for daily mean fields of geopotential height at 1000 (Z1000) and 700 hPa (Z700) and horizontal wind at 700hPa (using its zonal U and meridional V components), over the period 1979–2019.

Daily precipitation data for ANZ come from the National Institute of Water and Atmospheric Research (NIWA) Virtual Climate Station Network (VCSN). Data coverage for the NIWA VCSN [*Tait and Turner*, 2005; *Tait et al.*, 2006, 2012] is available from 1972 to present for 13 daily climate variables on a 5 x 5 km grid covering the country. The approach to generate the NIWA VCSN uses a thin-plate smoothing spline model for spatial interpolation between in situ station data, incorporating two location variables (latitude and longitude) and a third "pattern" variable. For precipitation (Fig. 1c), a digital version of an expert-guided 1951–80 mean annual rainfall isohyet map was used as the pattern variable as a way to represent orographic influences that arise from prevailing circulation interacting with mountainous terrain (Fig. 1d). VCSN data yield biased estimates of precipitation, especially in the most elevated parts of the country where the density of rain-gauge and weather stations is much reduced [*Tait et al.*, 2012; *Mason et al.*, 2017; *Jobst et al.*, 2018].

2.2 Methods

As in P21, this study uses the WT classification performed by K2K over the ANZ sector. The corresponding 12 WTs, originally based on 12-hourly maps of Z1000 derived from NCEP/NCAR reanalyses [*Kalnay et al.*, 1996], are updated here using ERA5 daily ensemble fields. Two WT time distributions are therefore considered, the original WT classification based on NCEP/NCAR timing, and the redefined distribution obtained by ascribing each day of each member based on ERA5, over the period 1979-2019, to its nearest type centroid. These two type definitions are seen to differ, with roughly 35% of the days of the period not being ascribed to the same WT. However, the composite mean fields are very similar, because day swaps between types are associated with similar patterns that differ only in the location of ACAs. The latter are expected to be more precisely defined by ERA5 data due to its much higher spatial resolution. Except when otherwise indicated, all results and conclusions discussed below can be obtained with both WT distributions. More details and a comparison between both WT timings are given in P21.

In addition to the partitioning into 12 discrete WTs, we reuse here the descriptors from P21 that monitor the location and intensity of the main ACAs associated with each type. These descriptors are derived from Z1000 daily anomalies (noted Z1000'), after removing the mean annual cycle, and are calculated over the larger domain shown in Fig. 1a. Three groups of WTs are formed, depending on the presence or absence of regional extremes of Z1000' [P21; Table 1]. The "Low" group has only one such extreme, consisting of a regional minimum of Z1000' denoting an atmospheric trough. Conversely, the "High" group only includes a regional maximum of Z1000', indicative of an atmospheric ridge. The "Gradient" group has both

extremes. The descriptors defined in P21 qualitatively differ from one group of WTs to another. For the “Low” group, three metrics depict the intensity of the low, corresponding to the minimum Z1000' value within the whole domain (MinZ'), and its corresponding latitude and longitude (Lat, Lon) that define its location. The “High” types use the same metrics, but applied to the Z1000' maximum to define the high ACA. The “Gradient” types use both metrics, with additional ones used to depict the relative position and differences between both ACAs. This provides the difference between Z1000' maximum and minimum ($Diff_{Z'}$), the latitudinal and longitudinal differences in their locations ($Diff_{Lat}$, $Diff_{Lon}$), and finally the slope of the geopotential height gradient, defined as $Grad = Diff_{Z'}/\sqrt{Diff_{Lat}^2 + Diff_{Lon}^2}$. All descriptors are quantitative and thus help address one of the main weaknesses of the WT approach, which is in discretizing naturally continuous climate variability [P21].

The AR catalogue is developed from the Guan and Waliser [2019] Tracking Atmospheric Rivers Globally as Elongated Targets (tARget) algorithm, version 3. AR occurrence is assessed for each grid cell individually and the passage of each AR object (over multiple timesteps) is considered both as a series of contiguous timesteps, and as one event with the day of maximum IVT [*Prince et al.*, 2021b], depending on the AR variables (Table 2). AR objects are detected from ERA-Interim reanalysis [*Dee et al.*, 2011] between 1979 and 2019 (40 years) using 6-hourly IVT at 1.5° resolution. The characteristics of the ARs are used throughout this study, specifically the magnitude of the moisture flux in the meridional and zonal direction, the duration of the event, and the maximum total moisture flux throughout the event (Table 2). The relatively narrow landmass New Zealand, situated in the midlatitudes, allows for ARs to make landfall on all coastlines [*Prince et al.*, 2021a]. This setup is unique and requires additional consideration, especially when considering ARs that may cause impacts on the eastern side of the country [*Prince et al.*, 2021a]. To account for the landfalling direction of the AR, only ARs which have IVT directed from the ocean onto land are considered (a restriction which is explored in the Supplementary Material; filtering directions are shown in Fig. 4). This leads to the exclusion of many ARs that pass over the eastern side of the country since they made landfall on the western coast and passed over the Southern Alps, rather than making landfall on the east coast. This technique is an extension of the Guan and Waliser [2015] landfall detection which identifies the landfall location based on the presence of ocean upwind of where an AR intersects a coastline, however our method considered for each grid cell individually here rather than for the entire AR object. The importance of such filtering is addressed in later sections.

3. Co-occurrence between Atmospheric Rivers and Weather Types

The diagonals in Figure 3 show the number of daily AR detections for each of the 17 grid-points surrounding ANZ (Fig. 1b). They confirm the results of Prince et al. [2021a], who depict very few events landfalling over the eastern coasts of both islands (as did for instance a strong AR event in May 2021 that causes heavy rainfall and floods in these relatively flat regions). This contrasts with the frequent AR detections for the grid-points aligned along the western parts of the country, especially near the West Coast of the South Island of ANZ where a sharp topographic barrier (Fig. 1d) enhances AR influence on precipitation [*Kingston et al.*, 2016; *Reid et al.*, 2021; *Shu et al.*, 2021].

Other values (out of the diagonals) in Fig. 3 shows the count of AR days co-occurring in the two corresponding grid-points. Results show that detected AR events are quite large and often co-occur over several grid-points, especially (i) along the West Coast of the South Island, and (ii) over the northern part of the North Island, and to a lesser extent, (iii) near the Cook Strait between the two main islands. Interestingly, this third region also shows frequent co-variability with the two other blocks located further south and north, although the latter show very few synchronous detections. Similarly, there are very few events that co-occur in grid-points with contrasted terrain exposure (i.e., orientation of the coastline: for instance, the opposite coasts of the South Island). This is a consequence of the filtering applied to ARs based on their angle (Sect. 2.2) to account for the quite small size of ANZ (unfiltered results are shown in Supp. Fig. 1: the resolution of reanalyses may be too coarse to account for the sharp contrasts in terrain exposure in ANZ, unfiltered results are therefore likely to produce AR events found simultaneously in both coasts of the country). The few events landfalling on the eastern parts of ANZ also seem to show weaker co-variability between adjacent grid-points, suggesting smaller AR sizes.

Previous studies already analyzed the association between ARs and the 12 WTs obtained by K2K [*Cullen et al.*, 2019; *Porhemmat et al.*, 2021b; *Kingston et al.*, 2022]. However, they mostly considered the AR events leading to major snowfall / ablation or floods. Therefore, previous work mainly focused on the Southern Alps region, where AR development is most frequent [Fig. 3; *Prince et al.*, 2021a; *Marquardt Collow et al.*, 2022]. A general assessment of the association between AR occurrence and WT, and how these relationships vary from one region of ANZ to another, remains to be established. This is the aim of Figure 4. Supplementary Figures 2 replicates the same analysis without removing AR events based on their angle. Both figures consider the original definition of the WTs, following the work of K2K and based on NCEP/NCAR reanalyses, but also their redefinition using ERA5 higher-

resolution data [P21]. This is because both methodologies led to non-negligible differences (roughly 35% of the days being ascribed to a different WT on period 1979-2019), hence the need to characterize the reanalysis-dependency of our conclusions.

Our results first confirm the main conclusions obtained in the aforementioned studies. For the western but also most of the northern parts of ANZ, most AR events occur during the T type, which consists in a low-pressure system located over, on average, south of ANZ, and favoring enhanced westerly winds north of the trough (Fig. 2). Thus, this type is generally associated with enhanced westerly winds. It is likely to be associated with AR events for all regions of ANZ considered in Fig. 4, albeit its very variable importance from one grid-point to another.

The relationships between ARs and WTs are even more region-dependent for all other WTs. Generally speaking, AR events landfalling in any region of ANZ tend to occur more frequently during the WTs that act to direct atmospheric fluxes and circulation towards that particular region. This is for instance the case for type W (broadly similar to T but shifted to the south: Fig. 2) over the southwestern parts of the country, HNW and SW (both favoring southerly anomalies) for the southernmost grid-points, or TNW (favoring northwesterly anomalies over the north of ANZ: Fig. 2) for the northernmost grid-points (#12 to #16: Fig. 4) or HE (broadly similar but with ACAs shifted towards the south) for the grid-points aligned along the west coasts of the islands. These side oppositions are, logically, less marked when AR events are not filtered depending on their angle (Supp. Fig. 2).

Fig. 4 also confirms that the original NCEP/NCAR definition of the WTs and their ERA5 redefinition sensibly differ. The case of type W, already identified as associated with large reanalysis-dependency in P21, can also be mentioned here and leads to dissimilar WT contributions to AR occurrences, especially over the southern and western parts of ANZ (Fig. 4). Other non-negligible differences can be found with types NE (e.g., grid-point #7), or TSW (grid-points #5 and #7), the other types showing strong dissimilarities between both reanalyses (e.g., H, HW and SW: P21) being more rarely associated with AR development.

Finally, another major result shown in Fig. 4 is that, in all regions of ANZ, AR events are likely to occur during very different and contrasted synoptic configurations, as materialized here by the WTs. The largest contribution of a given WT is 33.6% (for the T type in region #9), showing that the most favorable type is, at best, only responsible for a third of all AR events occurring in a given region. Hence, ARs landfalling in any part of ANZ can result from very different and diverse synoptic types, and these types differ from one region of ANZ to another. The main

common result across all regions is that WTs promoting stronger onshore winds are those generally favoring the largest AR occurrences.

4. AR and WT combined and separate influences on precipitation

4.1 Precipitation Anomalies

The effects of landfalling ARs on precipitation in ANZ has already been assessed before [*Reid et al.*, 2021; *Shu et al.*, 2021], as have been those of WTs *[K2K; Renwick, 2011; Pohl et al. 2022*: revised]. Here, we attempt to consider how their respective influences combine, that is, we analyze precipitation anomalies by WT and depending whether or not these WT days also correspond to AR occurrences. This could contribute to explain part of their strong internal variability, as pointed out by P21. Unlike previous work, we base our analyses on the 5-km resolution VCSN product, thereby allowing for a more detailed and precise assessment of the spatial coherence of rainfall variability patterns associated with WTs and ARs.

Fig. 5 shows the daily precipitation anomalies during the five WTs most favorable to AR development (Fig. 4), during all days ascribed to the corresponding WT, and then by differentiating NoAR days from AR days. The latter are further separated into two groups, by considering the case of the particularly strong AR events (corresponding to the top 10% ARs according to their associated IVT). Here, the case study retained is a grid-point located near the West Coast of the South Island of ANZ (#6: Fig. 1b; Fig. 4), identified as the region where ARs are responsible for the largest rainfall amounts, and may cause significant damage and environmental impacts [*Prince et al.*, 2021a; *Shu et al.*, 2021]. In order to focus on more inhabited regions and also to illustrate the diversity and regional dependency of our results, these analyses are duplicated for the southernmost (#0) and northernmost (#16) grid-points (Supp. Fig. 3).

Results (Fig. 5, first column) reveal very strong differences in precipitation anomalies, from one type to another, thereby corroborating previous work [K2K; *Renwick*, 2011; *Jiang et al.*, 2013]. Most WTs favorable to AR landfall along the West Coast are associated, on average, with wet anomalies there. The only exception is the NE type, which recurrently co-occurs with ARs (especially according to the ERA5 redefinition of the WTs: see Fig. 4) and tends yet to correspond, on average, to weaker than normal daily rainfall west of the main divide. In other regions of ANZ, these regimes produce precipitation anomalies of much weaker amplitude,

but of contrasted sign (e.g., drier than normal over the North Island for types W and HE, while the reversed sign prevails along the western slopes of the main reliefs for types T and TNW).

This average picture of WT influence on precipitation anomalies conceals strong internal variability, part of which can be related to AR development. The same WTs, when they do not co-occur with AR events, are indeed related to generally drier conditions over ANZ, and more particularly along the West Coast region (Fig. 5, second column). While wet anomalies are just weakened for the W type (when not accompanied by any AR), those associated with types T and TNW are dramatically smaller and barely exceed the statistical significance bound. The dry conditions recorded there during the NE type are enhanced in the absence of AR, and the wet conditions linked with the HE type change sign when no AR development occurs. In sharp contrast, the same five types all show much wetter conditions, over the West Coast, during AR landfall (third column), and the wet conditions recorded there are even larger during the 10% strongest AR events (fourth column). Hence, AR occurrence is a key parameter to consider to explain the internal diversity of precipitation amounts within each WT. The case of type NE is particularly striking, as this WT is drier than normal on average (–10 to –15 $mm.day^{-1}$) and even more clearly when not associated with ARs (–20 to –25 $mm.day^{-1}$), but it is significantly wetter than normal during moderate ARs (+15 to +20 $mm.day^{-1}$) and strong ARs (+ 50 to +70 $mm.day^{-1}$). This result show that within-type diversity cannot be considered as negligible, when analyzing daily precipitation across ANZ [Pohl et al. 2022, revised].

Although these general conclusions are qualitatively verified for all grid-points around ANZ, the magnitude of the differences between AR and NoAR days is much reduced, quantitatively, over most other regions of the country. This is because precipitation amounts and variability is largest over the West Coast, owing to its sharp topographic barrier almost perpendicular to the dominant westerly winds. Other regions may also show weaker spatial coherence in the precipitation anomaly fields linked to WT and AR occurrences. In the Supplementary Materials, we discuss this issue for the southernmost and northernmost regions of ANZ, retained as case studies.

4.2 Precipitation Extremes

Because of the strong spatial contrasts in precipitation amounts, and their variability, across ANZ, considering the mere amplitude of anomalies as done in Fig. 5 is not convenient to assess to which extent WTs and ARs contribute (jointly or separately) to precipitation extremes. Hence, with Figure 6, we explore to which extent ARs, and their most favorable WTs, are over-represented in daily precipitation extreme occurrences, and could therefore be

considered as one of their main drivers. For each occurrence of a favorable WT (either associated or not with an AR event) in the West Coast of the South Island, we calculate the rank of the corresponding day, in terms of daily precipitation anomalies, for all grid-points of the VCSN fields and across ANZ. Figure 6a shows the median and Figure 6b the 90th percentiles of the corresponding samples of days. Only values above the median and 90th percentiles are represented, since they can be interpreted as a statistical overrepresentation of the corresponding WTs, landfalling ARs, or their association. These analyses, duplicated for all 17 landfalling locations around ANZ (see Fig. 1b), show strong regional-dependency: Supp. Figs. 4-5 illustrate this result with the cases of southernmost and northernmost grid-points #0 and #16.

When considering their total occurrences, these WTs all tend to promote daily extremes in the West Coast region, except type NE (identified as anomalously dry on average there: Fig. 5). Type HE shows the weakest overrepresentation of precipitation extremes, and was also previously identified as conducive to anomalously wet conditions on the West Coast, but with magnitudes weaker than the remaining three types. During the occurrences of these five WTs, the probability of a daily precipitation extreme strongly decreases for the NoAR category (Fig. 6). Although this conclusion holds for all five WTs, it is particularly true for the “driest” types HE and NE, not promoting any increased probability of extreme in the absence of AR events. The situation strongly differs, for the West Coast region, when considering the co-occurrence of these types with moderate, and even more clearly, strong ARs. Daily precipitation extremes there are much favored by the co-occurrence of these selected WTs and ARs: for types W, T and TNW, 50% of corresponding moderate ARs bring precipitation that rank in the top 10% of daily anomalies, and 50% of the corresponding strong ARs in the top 5% (Fig. 6a). Similarly, 10% of the moderate and strong AR events bring daily precipitation anomalies above the 97th and 99th percentiles, that is, that rank in the top 3% and 1%, respectively (Fig. 6b). Although ranks tend to be slightly weaker for AR events occurring during type HE, the spatial pattern of daily precipitation is very similar to the three aforementioned WTs, and mostly consists in a sharp contrast corresponding to the major topographic barrier formed by the Southern Alps mountain range. Hence, much drier conditions are found along the eastern coast of the South Island, corresponding to the flatter coastal regions of Canterbury and Otago. In the case of strong ARs, however, wet conditions tend to extend further towards the east, and most of ANZ experiences heavy precipitations. This suggests that the strongest ARs, in terms of moisture transport, cause large-scale precipitation events, with a weaker sheltering effect of topography. Thus, the spatial extension of the heavy precipitation zone (as extracted here based on those AR events that hit the West Coast of the South Island) recurrently reached

437 the central and even northern parts of the North Islands, the eastern parts of the South Island
438 in the other side of the main divide, and the southernmost locations of the country.
439
440 The case of type NE is different from all others, because this WT is associated with wet
441 conditions in the eastern parts of the two main islands of ANZ (Fig. 5). It is rarely associated
442 with large amounts west of the Alps except during moderate and even, more markedly, strong
443 ARs. In the latter cases, the region influenced by ARs seem to encompass both sides of the
444 main mountain ranges. The northern tip of ANZ also experiences intense to extreme
445 precipitation records during the combined occurrences of this type and ARs landfalling on the
446 West Coast of the South Island. This suggests rain-bearing systems and atmospheric
447 circulation anomalies quite different from the other WTs selected here. This question is
448 addressed below.
449
450 This section confirmed that AR events are responsible for heavy precipitation amounts in ANZ,
451 and are likely to strongly modulate the influence of the 12 WTs of K2K on precipitation
452 variability and amounts. Intense to extreme daily precipitation anomalies tend also to occur
453 preferentially during ARs.
454
455
456 **5. AR and WT inter-relationships**
457
458 It seems reasonable to expect AR properties (Table 2) to be partly driven by the location and
459 intensities of synoptic ACAs [as is the case for Europe, the North Pacific and East Antarctica:
460 see *Eiras-Barca et al.*, 2018; *Fish et al.*, 2019; *Pohl et al.*, 2021b, respectively]. Here, ACAs
461 are themselves discriminated by the 12 discrete synoptic WTs and their associated
462 quantitative descriptors (Table 1). In this section, we assess how these two families of
463 atmospheric circulations are interrelated, over and near ANZ.
464
465 *5.1 Synoptic control on AR properties*
466
467 Figure 7 presents the statistical distribution of all AR properties, presented here as violin plots,
468 for each WT and for the West Coast region of the South Island. The same analyses for the
469 two most remote grid-points are shown in Supp. Fig. 6. Analysis of Fisher's test shown in Fig.
470 7 for all quantitative metrics (thus excluding AR directions) suggests that synoptic conditions,
471 monitored through the 12 WTs, strongly and significantly influence AR characteristics, with
472 estimated statistical significance exceeding the 99.99% ($p < 10^{-4}$). These statistics may be
473 biased by the large sample sizes, so that more qualitative analysis may be appropriate.

Figure 7 reveals that both zonal and meridional components of IVT, for these AR events reaching the western part of South Island, strongly differ from one WT to another. Although the zonal component is shifted towards positive values (denoting a westerly component that was expected at these latitudes), some WTs (namely, TNW, TSW, HSE and particularly NE: Fig.7) favor more balanced or more variables signs suggesting recurrent easterly advections. The meridional component similarly shows a shift towards negative values indicative of moisture transport from the lower latitudes, but some WTs (SW, HNW, HW) also correspond to ARs with a marked southerly component. These results are true when all timesteps of the AR lifecycles are considered, but also hold for the only maximum of moisture transport. Overall, when combined, these results show that the WTs have a strong influence on AR directions (Fig. 7). This conclusion is also true for other regions of ANZ (Supp. Fig. 6), although the filtering used here to select ARs coming only from the sea may also strongly decrease the statistical spread of AR directions, depending on the geometry of the coastline (Fig. 4; Supp. Fig. 6a).

Finally, WTs also modulate AR durations and their time-integrated total IVT. While types H, HNW, HW and R tend to coincide with the less persistent ARs (as shown by a median duration of just 6 hours, that is, the AR detection timestep), types TNW, W, HE and NE are associated with much longer AR events, as indicated both by their median duration (18h, that is, 3 detection timesteps) and largest values (reaching or exceeding 4 days, i.e. 96h or 16 detection timesteps). Time-integrated total IVT (and their WT-dependency) are very consistent with the duration, the longer events logically leading to larger moisture advections. These duration statistics of AR events embedded in WT sequences appear quite disconnected from the typical persistence of the WT sequences themselves, as assessed by K2K (his Figure 4): the most persistent WTs are not those conducive to the most persistent ARs. The latter are also 2 to 3 times shorter, suggesting that ARs preferentially develop within WTs in a vast majority of cases, rather than during the transition from one WT to another. Because of their weak persistence, AR events associated with more than one WT are rare, especially when WTs are defined at the daily timestep as done for this work.

The results discussed above generally hold for all grid-points shown in Fig. 1b and used for AR detection, in spite of a tendency for more persistent AR sequences over the northern parts of ANZ. Despite major differences in sample sizes (in terms of AR count and their association with synchronous WTs: Figs. 3-4), WT influence on AR properties appears strongly consistent from one region of ANZ to another (not shown).

5.2 Synoptic differences between AR and NoAR days

In addition to the relationship between WT and AR occurrence, do ARs influence WT synoptic patterns in return, and/or develop within synoptic patterns that may differ from the mean view of the WT, as obtained when merging all days? This hypothesis, if verified, (i) would be consistent with the strong within-type variability suggested in Section 4 and based on daily precipitation fields, (ii) would be in line with the results of Eiras-Barca et al. [2018] over the northern mid-latitudes, or Pohl et al. [2021b] over the southern high latitudes. It is therefore tested below.

Figure 8 shows changes in the regional-scale circulation (geopotential height and horizontal wind anomalies at 700hPa) during the five WTs most favorable to ARs in the West Coast, and separates NoAR days from moderate and strong AR events. Both definitions of the WTs are used, because they lead to slightly different results (both in terms of preferential associations between WTs and ARs, Fig. 4, and within-type differences). Supplementary Figures 7 and 8 show the same results for the southernmost and northernmost regions of ANZ, respectively.

Daily geopotential and circulation anomalies associated with these WTs when not co-occurring with ARs are similar to the average pattern of these types (Figs. 8 and 2). They are also generally quite consistent for both WT definitions (Figs. 8a-b), even though ACAs (and more particularly the negative ones, indicative of atmospheric troughs) tend to reach larger intensities using the newer ERA5 distribution. This is probably due to the more detailed and accurate resolution of the ridges and troughs in ERA5, in line with its finer grids. These WTs favor moisture transport towards the West Coast of the South Island, either from the west or northwest (for types W, HE and TNW) or southwest (T).

Type NE, being associated with northeasterly anomalies west of ANZ, is once again quite different from the other WTs selected here: this cyclonic circulation explains its strong influence on precipitation amounts even over the North Island (Section 4.1). Within-type differences between NoAR and AR days are weaker (half the magnitude) than the mean departures from the mean annual cycles during the overall occurrences of this type (Fig. 8). This indicates that, even during AR days, this WT is still well characterized by its main synoptic-scale specific patterns.

A more general statement is that such within-type differences between NoAR and (moderate-intensity) AR days are remarkably similar across the types, and do not appear to be directly related to the mean anomaly patterns of the types. For all WTs, they consist in a dipole of

548 geopotential height, with positive differences northeast of ANZ, and negative ones west of it.
549 This dipole is thus associated with a stronger northwesterly component of the winds, which
550 favors moisture transport towards the West Coast of the South Island, perpendicularly to the
551 main topographic barrier of the Alps. Albeit their weaker magnitudes, these differences are
552 very consistent with the AR patterns landfalling there, as discussed in the literature [*Kingston*
553 *et al.*, 2016, 2022; *Cullen et al.*, 2019; *Little et al.*, 2019; *Prince et al.*, 2021a; *Reid et al.*, 2021;
554 *Shu et al.*, 2021]. Within-type differences are also larger according to the original NCEP/NCAR
555 definition of the WTs (Fig. 8b), especially the negative geopotential height differences located
556 west or southwest of ANZ. Through geostrophy, this leads to increased differences in both
557 horizontal components of the wind, and thus enhanced northwesterly wind reaching the West
558 Coast region. This favors moisture transport from the lower latitudes of Tasman Sea towards
559 ANZ. Supplementary Figure 8 confirms these conclusions for other parts of ANZ, although the
560 location and orientation of the geopotential dipole changes, so that the resulting fluxes reach
561 the landfalling region with stronger westerly (for the southern regions) or
562 northerly/northwesterly components (for the northern regions of ANZ).
563
564 In contrast with the marked differentiation between NoAR and moderate AR days, differences
565 between strong and moderate ARs seem much noisier and less coherent, spatially and
566 physically. This suggests that the intensities and location of the main ACAs could have limited
567 control on the strength of landfalling ARs, as inferred by their IVT. Thus, the strength of the
568 ARs could possibly be more related to the moisture content of the air mass, than stronger
569 synoptic ACAs.
570
571 By analyzing anomalies of specific humidity and moisture fluxes around ANZ, Supplementary
572 Figure 9 aims at exploring this issue. It generally confirms the conclusions of previous work
573 concluding that southerly anomalies advect dry air towards ANZ, northerly fluxes having an
574 opposite effect [e.g., *Pohl et al.*, 2021b]. Furthermore, it points out that the air mass contains
575 significantly more humidity during strong ARs than moderate ones, especially north of ANZ.
576 Differences between NoAR and moderate ARs on the one side, moderate ARs and strong
577 ARs on the other side, have about the same magnitude as the transient anomalies associated
578 with the WTs.
579
580 Overall, our results suggest that synoptic conditions have strong importance for AR
581 development and for shaping their location and angle, while corresponding IVT seems to be
582 influenced by the available moisture content in the subtropical latitudes that can next be
583 advected southwards once the AR is formed. These results are verified for the northern
584 regions of ANZ, they still hold for the West Coast of the South Island, but air humidity from the

585 subtropics seems of little importance for the southernmost parts of the country (Supp. Fig. 9).
586 These regions also exhibit slightly different associations with WTs during strong vs. moderate
587 ARs, with type TNW (associated with southwesterly anomalies: Fig. 2) tending to promote
588 strong IVT conducive to major AR events. The different moisture sources, from higher
589 latitudes, that could affect this part of the country, corroborate the results of Bennet and
590 Kingston [2022] on the spatial patterns of IVT in ANZ, and are also coherent with *Reid et al.*
591 [2022] who obtained similar results for Australia. More detailed assessment of moisture
592 sources is now needed, e.g. through lagrangian approaches, but this is not our scope here.
593
594 *5.3 Interactions between AR properties and synoptic configurations*
595
596 Section 5.1 discussed how synoptic configurations, as materialized by the 12 WTs, modify AR
597 features. Section 5.2 further established that synoptic configurations themselves differ
598 depending on the presence, absence, and for some cases, strength of the AR events. Here,
599 we attempt to reconcile these views, and analyze these interactions in a unified way. Figure 9
600 shows how AR attributes (as summarized in Table 2) relate to the synoptic descriptors of ACAs
601 (as summarized in Table 1). These analyses are done for each day ascribed to the five more
602 favorable types promoting the largest numbers of ARs reaching the West Coast region.
603 Supplementary Figures 10 and 11 duplicate these results for the southernmost and
604 northernmost regions of ANZ, respectively.
605
606 Whatever the definition of WTs, Fig. 9 indicates that the intensity of atmospheric ridges is
607 significantly related to changes in AR properties. This is especially true for types TNW, W and
608 HE. The T type has no positive ACA: it mostly relates to changes in AR characteristics through
609 the latitude, and to a lesser extent, the intensity, of its main atmospheric trough. In spite of the
610 statistical significance of some associations between within-type diversity and AR properties,
611 the common variance between corresponding couples of descriptors remains low. This may
612 be due (i) to the large sample size (exceeding 3000 days for grid-point #6: Fig. 3), and/or (ii)
613 to the fact that we are considering here residual variability, the main changes being likely
614 associated with differences between WTs (Section 5.1). Nevertheless, this still suggests that,
615 under a given synoptic context, AR diversity, from one day or event to another, cannot be
616 interpreted as simple linear functions of the location and intensities of ACAs. These general
617 conclusions and results, including a significant but still moderate role of the intensity of
618 atmospheric ridges, are also verified for other regions of ANZ (Supp. Figs. 10-11).
619
620 How within-type diversity could relate, physically, to changes in AR properties, cannot be
621 assessed based on correlation analyses. The negative correlation between ridge intensities

and moisture transport may also seem counter-intuitive, strong ridges or blockings being mentioned in the literature as a favorable condition for moisture transport channeling and, thus, AR development [*Pohl et al.*, 2021c]. Hence, Figure 10 shows composites of the opposite phases of the synoptic descriptors found in Fig. 9 to influence AR properties. The composite approach used here (based on the 20th and 80th percentiles of each descriptor), discussed in P21, does not assume that relationships are linear, as do the correlation analyses of Fig. 9. Qualitatively similar results could be obtained with other percentile values (not shown).

The W type is formed by a strong negative ACA southwest of ANZ and a weaker positive one north it, that channel westerly winds towards the country (Fig. 10), hence its strong contribution to AR occurrences for parts of ANZ (Fig. 4). It is the positive ACA that mostly acts to modify AR properties, with larger ridge intensities corresponding to reduced moisture transport (Fig. 9). Strongest ridges actually correspond to a Z1000 pattern that sensibly differs from the canonical view of that WT, with an alternation of atmospheric waves in the mid-latitudes that is associated with stronger sinuosities of the westerlies. This could correspond to generally weakened winds, hence the decreased moisture transport. Similar results are obtained with type TNW: here, particularly strong ridges clearly increase the transient wave component of mid-latitude circulation, as compared to the weaker ridge occurrences associated with this type. As a result, corresponding AR events exhibit a weaker zonal moisture transport.

The T type is the most favorable one for AR development for many parts of ANZ (Fig. 4). It shows a single negative ACA consisting in a trough (hence its name) located near or just south of ANZ. The negative correlations between IVT on the one side, and the intensity and latitude of the troughs on the other side, imply that stronger troughs (larger negative values of geopotential height anomalies), and/or southernmost locations, both favor increased moisture advections linked to ARs. Indeed, both types of configurations increase westerly winds north of the trough (Fig. 10), leading to stronger atmospheric fluxes meeting the coasts and mountains of ANZ. Similar mechanisms also prevail for the troughs associated with types W, TNW and HE, albeit their weaker correlations (Fig. 9).

This section pointed out how synoptic ACAs, by modulating the westerly wind speeds, can modify AR-associated IVT towards the West Coast of ANZ. These relationships remain of moderate strength, despite their statistical significance. A possible reason is that our analyses are only based on atmospheric dynamics, hence the need to consider air humidity and to identify moisture sources in future work.

6. Discussion & Conclusion

In this work we analyze relationships between the 12 weather types of Kidson (2000), defined over the Aotearoa New Zealand (ANZ) sector, and atmospheric rivers (ARs) landfalling in different parts of ANZ. Focus is given on inter-type variability, and how differences in the weather patterns around ANZ act to modify AR properties (angle, water vapor transport, …), as well as within-type diversity, and how it relates to AR variability. To that end, two series of descriptors are used: they monitor, on the one hand, the intensity and location of main atmospheric centers of action (ACAs) associated with the WTs, and on the other hand, the angle, duration and moisture transport associated with the ARs. Analyzing jointly the co-occurrences of WTs, ARs, and their respective descriptors, allowed us to explore how they are interrelated, thereby complementing the more usual analyses of AR probability depending on the synoptic context, or the relative contribution of each WT to overall AR occurrences. The relative importance of inter-type vs. within-type diversity is also addressed from a precipitation point of view, by assessing the combined and separate influence of WTs and ARs on daily amounts across ANZ. The case of precipitation extremes is considered, ARs being recurrently identified as a key driver of such precipitation excesses.

Our main results can be summarized as follows.

— AR occurrences display clear preferential associations with a few WTs, and these associations are strongly region-dependent across ANZ. The most favorable WTs are, quite logically, those that act to direct moisture fluxes towards the country. However, a more meaningful result is that, for a given region, the most favorable WT is responsible, at most, for only a third of overall AR events. Generally, three or four WTs can be identified as the main drivers of ARs, for a given region of interest. These WTs strongly differ from one part of ANZ to another, the most recurrent favorable types being those that promote increased westerly, or a marked northwesterly component, to the regional atmospheric circulation.

— Within-type and inter-event variability and diversity is large, both for ARs and WTs. Some AR attributes are strongly modulated by WTs. This is especially the case for their angle, but their persistence also differs between WTs.

— When co-occurring with AR events, the WTs tend in return to show changes in the location of their main ACAs, that act to deviate the winds towards ANZ. ACAs do not appear to be significantly more intense during the strongest ARs, that is, those associated with the largest moisture transport. However, the air mass is significantly more moist during the latter events, especially north of ANZ. While AR occurrence, location and angle are favored and largely driven by synoptic-scale variability, vapor transport appears more tightly related to lower-layer specific humidity (especially for the northern regions of ANZ, connected with subtropical

696 regions during major AR events). For the southern regions, key features involve the velocity
697 of mid-latitude westerly winds, while links with the subtropical latitudes are weaker.
698 — Such within-type variability has also major consequences for precipitation variability, and
699 for the occurrence of daily extremes. The composite mean anomaly patterns of precipitation
700 conceal major changes between NoAR and AR days. Strong AR events (in terms of moisture
701 transport) also differentiate from moderate events. Their implication is particularly strong for
702 wet extremes: half of moderate (strong) ARs produce precipitation that rank in the top 10%
703 (5%) anomalies. The same WTs only yield weak anomalies when not co-occurring with ARs,
704 or even, in some cases, anomalies of opposite sign (i.e., drier than normal).
705
706 This study illustrated how WTs can drive and/or modify AR development and their associated
707 attributes. The reverse relationship remains still unclear to date. Another major aspect to
708 consider could then be to assess to what extent ARs influence WTs in return, that is, modify
709 the strength and/or location of their main ACAs. Differentiated evolutions of ACAs would be
710 consistent with larger latent heat release during ARs, increasing cyclogenesis through
711 differential diabatic heating profiles [*Madonna et al.*, 2014; *Woollings et al.*, 2018; *Terpstra et*
712 *al.*, 2021]. A more detailed analysis of the life cycle of these ACAs could be performed, for
713 instance using analogues, in order to determine whether they evolve differently under AR and
714 NoAR conditions.
715
716 Our results suggest that the available moisture in the subtropical regions east of Australia
717 could be a key variable to include in future studies. The question of the moisture sources for
718 ARs could be addressed e.g. by using back trajectories or lagrangian approaches - as already
719 indicated by Kingston and McMecking [2015] for flooding events in the Southern Alps. Latent
720 heat fluxes at the interface between atmosphere and oceans (e.g. over Tasman and Coral
721 seas) or continent (Australia) are intuitive candidates that could favor increased moisture in
722 the lower troposphere, more likely to lead to AR formations.
723
724 Last but not least, this work solely analyzed the synoptic scale, at which both WTs and ARs
725 develop and interact. However, in the mid-latitudes of the Southern Hemisphere, atmospheric
726 circulations strongly varied and evolved since the early 20th century [*Thompson and Solomon*,
727 2002; *Fogt et al.*, 2009; *Polvani et al.*, 2011], at various timescales spanning from interannual
728 to multi-decadal [*L'Heureux and Thompson*, 2006; *Oliveira et al.*, 2013]. Such changes are
729 further projected for the future decades under ongoing climate change [*Arblaster et al.*, 2011;
730 *Perlwitz*, 2011; *Zheng et al.*, 2013]: WTs [*Parsons et al.*, 2014; *Gibson et al.*, 2016] and ARs
731 [*Espinoza et al.*, 2018; *Ma et al.*, 2020] themselves will also show gradually-evolving properties
732 under increasing greenhouse gas concentrations. How these lower frequencies affect both

WTs and ARs over the region is a major question to address. How changes in the atmospheric and climate dynamics [*Sansom and Renwick*, 2007] could combine their influence to the so-called Clausius-Clapeyron scaling [*Betts and Harshvardhan*, 1987; *Trenberth et al.*, 2003; *Kharin et al.*, 2007; *Pall et al.*, 2007; *O'Gorman and Schneider*, 2009; *Muller et al.*, 2011; *Westra et al.*, 2014] to modify precipitation amounts, especially wet extremes at daily and sub-daily timescales, is another subject of concern for the local societies and territories. Further work is strongly needed to cast light on these subjects and help adapt to ever increasing changes in the local, regional and global climate.

Acknowledgments

This study is a contribution to the sea4seas project funded by the University of Burgundy. Nicolas Fauchereau was supported by the NIWA Strategic Science Investment Fund project ''Climate Present and Past''. The authors thank Prof. James Renwick for making the original Kidson type distribution available and for updating it over the recent years. All analyses were made with python (libraries numpy, pandas, scipy, sklearn, math, matplotlib, cartopy, seaborn, netCDF4), the developers of which are thanked. Calculations were performed using HPC resources from DNUM CCUB (Centre de Calcul de l'Université de Bourgogne).

CRediT authorship contribution statement

Conceptualization, Methodology, Software: Benjamin Pohl
Formal Analysis: Benjamin Pohl, Hamish Prince, Daniel Kingston, Jonathan Wille, Nicolas Cullen, Nicolas Fauchereau
Data curation: Hamish Prince, Nicolas Fauchereau, Benjamin Pohl
Visualization: Benjamin Pohl, Hamish Prince
Writing - Original Draft: Benjamin Pohl, Hamish Prince, Jonathan Wille, Daniel Kingston, Nicolas Cullen
Funding Acquisition: Benjamin Pohl, Nicolas Fauchereau

Data Availability Statement

ERA5 data can be retrieved from https://cds.climate.copernicus.eu/cdsapp#!/search?type=dataset&text=era5. The AR data are

available at https://ucla.box.com/ARcatalog. AR detection is based on the algorithm originally introduced in Guan and Waliser [2015], refined in Guan et al. [2018], and further enhanced in Guan and Waliser [2019]. Weather types and their descriptors [P21] are available at https://pohlben.files.wordpress.com/2022/02/ktdescriptors_era5.xlsx and https://pohlben.files.wordpress.com/2022/02/ktdescriptors_ncep.xlsx. VCSN data can be retrieved from the NIWA website at https://niwa.co.nz/climate/our-services/virtual-climate-stations.

References

Ackerley, D. et al. (2011), Using synoptic type analysis to understand New Zealand climate during the Mid-Holocene, *Clim. Past*, *7*(4), 1189–1207, doi:10.5194/cp-7-1189-2011.

Arblaster, J. M., G. A. Meehl, and D. J. Karoly (2011), Future climate change in the Southern Hemisphere: Competing effects of ozone and greenhouse gases, *Geophys. Res. Lett.*, *38*(2), L02701, doi:10.1029/2010GL045384.

Bennet, M. J., and D. G. Kingston (2022), Spatial Patterns of Atmospheric Vapour Transport and their Connection to Drought in New Zealand, *Int. J. Climatol.*, (March 2021), 1–21, doi:10.1002/joc.7554.

Betts, A. K., and Harshvardhan (1987), Thermodynamic Constraint on the Cloud Liquid Water Feedback in Climate Models, *J. Geophys. Res.*, *92*(D7), 8483–8485, doi:10.1029/jd092id07p08483.

Coggins, J. H., S. Parsons, and D. Schiel (2016), An assessment of the ocean wave climate of New Zealand as represented in Kidson's synoptic types, *Int. J. Climatol.*, *36*(6), 2481–2496, doi:10.1002/joc.4507.

Cullen, N. J., P. B. Gibson, T. Mölg, J. P. Conway, P. Sirguey, and D. G. Kingston (2019), The Influence of Weather Systems in Controlling Mass Balance in the Southern Alps of New Zealand, *J. Geophys. Res. Atmos.*, *124*(8), 4514–4529, doi:10.1029/2018JD030052.

Dee, D. P. et al. (2011), The ERA-Interim reanalysis : configuration and performance of the data assimilation system, *Q. J. R. Meteorol. Soc.*, *137*, 553–597, doi:10.1002/qj.828.

Dravitzki, S., and J. McGregor (2011), Extreme precipitation of the Waikato region, New Zealand, *Int. J. Climatol.*, *31*(12), 1803–1812, doi:10.1002/joc.2189.

Eiras-Barca, J., N. Lorenzo, J. Taboada, A. Robles, and G. Miguez-Macho (2018), On the relationship between atmospheric rivers, weather types and floods in Galicia (NW Spain), *Nat. Hazards Earth Syst. Sci.*, *18*(6), 1633–1645, doi:10.5194/nhess-18-1633-2018.

Espinoza, V., D. E. Waliser, B. Guan, D. A. Lavers, and F. M. Ralph (2018), Global Analysis of Climate Change Projection Effects on Atmospheric Rivers, *Geophys. Res. Lett.*, *45*(9), 4299–4308, doi:10.1029/2017GL076968.

Fauchereau, N., B. Pohl, and A. Lorrey (2016), Extratropical Impacts of the Madden–Julian Oscillation over New Zealand from a Weather Regime Perspective, *J. Clim.*, *29*(6), 2161–2175, doi:10.1175/JCLI-D-15-0152.1.

Fish, M. A., A. M. Wilson, and F. M. Ralph (2019), Atmospheric river families: Definition and associated synoptic conditions, *J. Hydrometeorol.*, *20*(10), 2091–2108, doi:10.1175/JHM-D-18-0217.1.

Fogt, R. L., J. Perlwitz, A. J. Monaghan, D. H. Bromwich, J. M. Jones, and G. J. Marshall (2009), Historical SAM Variability. Part II: Twentieth-Century Variability and Trends from Reconstructions, Observations, and the IPCC AR4 Models, *J. Clim.*, *22*, 5346–5365, doi:10.1175/2009JCLI2786.1.

Gibson, P. B., S. E. Perkins-Kirkpatrick, and J. A. Renwick (2016), Projected changes in synoptic weather patterns over New Zealand examined through self-organizing maps, *Int. J. Climatol.*, *36*(January), 3934–3948, doi:10.1002/joc.4604.

Guan, B., and D. E. Waliser (2015), Detection of atmospheric rivers: Evaluation and application of an algorithm for global studies, *J. Geophys. Res. Atmos.*, *120*, 12,514–12,535, doi:10.1002/ 2015JD024257.

Guan, B., and D. E. Waliser (2019), Tracking Atmospheric Rivers Globally: Spatial Distributions and Temporal Evolution of Life Cycle Characteristics, *J. Geophys. Res. Atmos.*, *124*(23), 12,523-12,552, doi:10.1029/2019JD031205.

Guan, B., D. E. Waliser, and F. M. Ralph (2018), An intercomparison between reanalysis and dropsonde observations of the total water vapor transport in individual atmospheric rivers, *J. Hydrometeorol.*, *19*(2), 321–337, doi:10.1175/JHM-D-17-0114.1.

Guan, K., B. Sultan, M. Biasutti, C. Baron, and D. B. Lobell (2015), What aspects of future rainfall changes matter for crop yields in West Africa?, *Geophys. Res. Lett.*, *42*(19), 8001–8010, doi:10.1002/2015GL063877.

Hersbach, H. et al. (2020), The ERA5 global reanalysis, *Q. J. R. Meteorol. Soc.*, *146*(730), 1999–2049, doi:10.1002/qj.3803.
Hoskins, B. J., M. E. McIntyre, and A. W. Robertson (1985), On the use and significance of isentropic potential vorticity maps, *Q. J. R. Meteorol. Soc.*, *111*(470), 877–946, doi:10.1002/qj.49711146602.
Jiang, N., K. N. Dirks, and K. Luo (2013), Classification of synoptic weather types using the self-organising map and its application to climate and air quality data visualisation, *Weather Clim.*, *33*, 52–75, doi:10.2307/26169737.
Jobst, A. M., D. G. Kingston, and N. J. Cullen (2018), High resolution precipitation fields for the Clutha catchment, *Weather Clim.*, *38*(1), 2–15, doi:10.2307/26779360.
Kalnay, E. et al. (1996), The NCEP/NCAR 40-Year Reanalysis Project, *Bull. Am. Meteorol. Soc.*, *77*, 437–471.
Kharin, V. V, F. W. Zwiers, X. Zhang, and G. C. Hegerl (2007), Changes in temperature and precipitation extremes in the IPCC ensemble of global coupled model simulations, *J. Clim.*, *20*(8), 1419–1444, doi:10.1175/JCLI4066.1.
Kidson, J. W. (2000), An Analysis of New Zealand synoptic types and their use in defining weather regimes, *Int. J. Climatol.*, *20*, 299–316.
Kingston, D. G., and J. McMecking (2015), Precipitation delivery trajectories associated with extreme river flow for the Waitaki River, New Zealand, *IAHS-AISH Proc. Reports*, *369*, 19–24, doi:10.5194/piahs-369-19-2015.
Kingston, D. G., D. A. Lavers, and D. M. Hannah (2016), Floods in the Southern Alps of New Zealand: the importance of atmospheric rivers, *Hydrol. Process.*, *30*(26), 5063–5070, doi:10.1002/hyp.10982.
Kingston, D. G., D. A. Lavers, and D. M. Hannah (2022), Characteristics and large-scale drivers of atmospheric rivers associated with extreme floods in New Zealand, *Int. J. Climatol.*, *42*(5), 3208–3224, doi:10.1002/joc.7415.
L'Heureux, M. L., and D. W. J. Thompson (2006), Observed relationships between the El-Niño-Southern oscillation and the extratropical zonal-mean circulation, *J. Clim.*, *19*(1), 276–287, doi:10.1175/JCLI3617.1.
Little, K., D. G. Kingston, N. J. Cullen, and P. B. Gibson (2019), The Role of Atmospheric Rivers for Extreme Ablation and Snowfall Events in the Southern Alps of New Zealand, *Geophys. Res. Lett.*, *46*(5), 2761–2771, doi:10.1029/2018GL081669.
Lorrey, A., A. M. Fowler, and J. Salinger (2007), Regional climate regime classification as a qualitative tool for interpreting multi-proxy palaeoclimate data spatial patterns: A New Zealand case study, *Palaeogeogr. Palaeoclimatol. Palaeoecol.*, *253*(3–4), 407–433, doi:10.1016/j.palaeo.2007.06.011.
Lorrey, A., P. Williams, J. Salinger, T. Martin, J. Palmer, A. Fowler, J.-X. Zhao, and H. Neil (2008), Speleothem stable isotope records interpreted within a multi-proxy framework and implications for New Zealand palaeoclimate reconstruction, *Quat. Int.*, *187*(1), 52–75, doi:10.1016/j.quaint.2007.09.039.
Lorrey, A., N. Fauchereau, C. Stanton, P. Chappell, S. Phipps, A. Mackintosh, J. Renwick, I. Goodwin, and A. Fowler (2014), The Little Ice Age climate of New Zealand reconstructed from Southern Alps cirque glaciers: a synoptic type approach, *Clim. Dyn.*, *42*(11–12), 3039–3060, doi:10.1007/s00382-013-1876-8.
Lorrey, A. M. et al. (2012), Palaeocirculation across New Zealand during the last glacial maximum at ~21 ka, *Quat. Sci. Rev.*, *36*, 189–213, doi:10.1016/j.quascirev.2011.09.025.
Ma, W., G. Chen, and B. Guan (2020), Poleward Shift of Atmospheric Rivers in the Southern Hemisphere in Recent Decades, *Geophys. Res. Lett.*, *47*(21), e2020GL089934, doi:10.1029/2020GL089934.
Madonna, E., H. Wernli, H. Joos, and O. Martius (2014), Warm conveyor belts in the ERA-Interim Dataset (1979-2010). Part I: Climatology and potential vorticity evolution, *J. Clim.*, *27*(1), 3–26, doi:10.1175/JCLI-D-12-00720.1.
Marquardt Collow, A. B. et al. (2022), An Overview of ARTMIP's Tier 2 Reanalysis Intercomparison: Uncertainty in the Detection of Atmospheric Rivers and Their Associated Precipitation, *J. Geophys. Res. Atmos.*, *127*(8), e2021JD036155,

doi:10.1029/2021jd036155.
Mason, E. G., S. Salekin, and J. A. Morgenroth (2017), Comparison between meteorological data from the New Zealand National Institute of Water and Atmospheric Research (NIWA) and data from independent meteorological stations, *New Zeal. J. For. Sci.*, *47*(7), doi:10.1186/s40490-017-0088-0.
Muller, C. J., P. A. O'Gorman, and L. E. Back (2011), Intensification of precipitation extremes with warming in a cloud-resolving model, *J. Clim.*, *24*(11), 2784–2800, doi:10.1175/2011JCLI3876.1.
O'Gorman, P. A., and T. Schneider (2009), Scaling of precipitation extremes over a wide range of climates simulated with an idealized GCM, *J. Clim.*, *22*(21), 5676–5685, doi:10.1175/2009JCLI2701.1.
Oliveira, F. M. N. M., L. M. V Carvalho, and T. T. Ambrizzi (2013), A new climatology for Southern Hemisphere blockings in the winter and the combined effect of ENSO and SAM phases, *Int. J. Climatol.*, *34*(5), 1676–1692, doi:10.1002/joc.3795.
Pall, P., M. R. Allen, and D. A. Stone (2007), Testing the Clausius-Clapeyron constraint on changes in extreme precipitation under CO2 warming, *Clim. Dyn.*, *28*(4), 351–363, doi:10.1007/s00382-006-0180-2.
Parsons, S., A. J. McDonald, and J. A. Renwick (2014), The use of synoptic climatology with general circulation model output over New Zealand, *Int. J. Climatol.*, *34*(12), 3426–3439, doi:10.1002/joc.3919.
Perlwitz, J. (2011), Tug of war on the jet stream, *Nat. Clim. Chang.*, *1*(1), 29–31, doi:10.1038/nclimate1065.
Pfahl, S., C. Schwierz, M. Croci-Maspoli, C. M. Grams, and H. Wernli (2015), Importance of latent heat release in ascending air streams for atmospheric blocking, *Nat. Geosci.*, *8*(8), 610–614, doi:10.1038/ngeo2487.
Pohl, B., A. Lorrey, A. Sturman, H. Quénol, J. Renwick, N. Fauchereau, and J. Pergaud (2021a), "Beyond weather regimes": Descriptors monitoring atmospheric centers of action-a case study for aotearoa new zealand, *J. Clim.*, *34*(20), 8341–8360, doi:10.1175/JCLI-D-21-0102.1.
Pohl, B., T. Saucède, V. Favier, J. Pergaud, D. Verfaillie, J.-P. Féral, Y. Krasniqi, and Y. Richard (2021b), Recent climate variability around the Kerguelen Islands (Southern Ocean) seen through weather regimes, *J. Appl. Meteorol. Climatol.*, *60*, 711–731, doi:10.1175/jamc-d-20-0255.1.
Pohl, B. et al. (2021c), Relationship Between Weather Regimes and Atmospheric Rivers in East Antarctica, *J. Geophys. Res. Atmos.*, *126*(24), e2021JD035294, doi:10.1029/2021JD035294.
Polvani, L. M., D. W. Waugh, G. J. P. Correa, and S.-W. Son (2011), Stratospheric Ozone Depletion: The Main Driver of Twentieth-Century Atmospheric Circulation Changes in the Southern Hemisphere, *J. Clim.*, *24*, 795–812, doi:10.1175/2010JCLI3772.1.
Porhemmat, R., H. Purdie, P. Zawar-Reza, C. Zammit, and T. Kerr (2021a), Moisture Transport during Large Snowfall Events in the New Zealand Southern Alps: The Role of Atmospheric Rivers, *J. Hydrometeorol.*, *22*(2), 425–444, doi:10.1175/jhm-d-20-0044.1.
Porhemmat, R., H. Purdie, P. Zawar-Reza, C. Zammit, and T. Kerr (2021b), The influence of atmospheric circulation patterns during large snowfall events in New Zealand's Southern Alps, *Int. J. Climatol.*, *41*(4), 2397–2417, doi:10.1002/joc.6966.
Prince, H. D., N. J. Cullen, P. B. Gibson, J. Conway, and D. G. Kingston (2021a), A climatology of atmospheric rivers in New Zealand, *J. Clim.*, *34*(11), 4383–4402, doi:10.1175/JCLI-D-20-0664.1.
Prince, H. D., P. B. Gibson, M. J. DeFlorio, T. W. Corringham, A. Cobb, B. Guan, F. M. Ralph, and D. E. Waliser (2021b), Genesis Locations of the Costliest Atmospheric Rivers Impacting the Western United States, *Geophys. Res. Lett.*, *48*(20), e2021GL093947, doi:10.1029/2021GL093947.
Ralph, F. M. et al. (2017), Atmospheric rivers emerge as a global science and applications focus, *Bull. Am. Meteorol. Soc.*, *98*(9), 1969–1973, doi:10.1175/BAMS-D-16-0262.1.
Ralph, F. M., M. D. Dettinger, M. M. Cairns, T. J. Galarneau, and J. Eylander (2018), Defining

943 “Atmospheric river" : How the glossary of meteorology helped resolve a debate, *Bull. Am.*
944 *Meteorol. Soc.*, *99*(4), 837–839, doi:10.1175/BAMS-D-17-0157.1.
945 Reid, K. J., S. M. Rosier, L. J. Harrington, A. D. King, and T. P. Lane (2021), Extreme rainfall
946 in New Zealand and its association with Atmospheric Rivers, *Environ. Res. Lett.*, *16*(4),
947 044012, doi:10.1088/1748-9326/abeae0.
948 Reid, K. J., A. D. King, T. P. Lane, and D. Hudson (2022), Tropical, Subtropical, and
949 Extratropical Atmospheric Rivers in the Australian Region, *J. Clim.*, *35*(9), 2697–2708,
950 doi:10.1175/jcli-d-21-0606.1.
951 Renwick, J. A. (2011), Kidson’s Synoptic Weather Types and Surface Climate Variability over
952 New Zealand, *Weather Clim.*, *31*, 3–23, doi:10.2307/26169715.
953 Salinger, M. J. et al. (2020), Unparalleled coupled ocean-atmosphere summer heatwaves in
954 the New Zealand region: drivers, mechanisms and impacts, *Clim. Change*, *162*, 485–
955 506, doi:10.1007/s10584-020-02730-5.
956 Sansom, J., and J. A. Renwick (2007), Climate change scenarios for New Zealand rainfall, *J.*
957 *Appl. Meteorol. Climatol.*, *46*(5), 573–590, doi:10.1175/JAM2491.1.
958 Shu, J., A. Y. Shamseldin, and E. Weller (2021), The impact of atmospheric rivers on rainfall
959 in New Zealand, *Sci. Rep.*, *11*(1), 1–11, doi:10.1038/s41598-021-85297-0.
960 Smith, W., C. Davies-Colley, A. Mackay, and G. Bankoff (2011), Social impact of the 2004
961 Manawatu floods and the “hollowing out” of rural New Zealand, *Disasters*, *35*(3), 540–
962 553, doi:10.1111/j.1467-7717.2011.01228.x.
963 Sodemann, H., and A. Stohl (2013), Moisture origin and meridional transport in atmospheric
964 rivers and their association with multiple cyclones, *Mon. Weather Rev.*, *141*(8), 2850–
965 2868, doi:10.1175/MWR-D-12-00256.1.
966 Tait, A., and R. Turner (2005), Generating multiyear gridded daily rainfall over New Zealand,
967 *J. Appl. Meteorol.*, *44*(9), 1315–1323, doi:10.1175/JAM2279.1.
968 Tait, A., R. Henderson, R. Turner, and X. Zheng (2006), Thin plate smoothing spline
969 interpolation of daily rainfall for New Zealand using a climatological rainfall surface, *Int.*
970 *J. Climatol.*, *26*(14), 2097–2115, doi:https://doi.org/10.1002/joc.1350.
971 Tait, A., J. Sturman, and M. Clark (2012), An assessment of the accuracy of interpolated daily
972 rainfall for New Zealand, *J. Hydrol. (New Zealand)*, *51*(1), 25–44.
973 Terpstra, A., I. V Gorodetskaya, and H. Sodemann (2021), Linking Sub-Tropical Evaporation
974 and Extreme Precipitation Over East Antarctica : An Atmospheric River Case Study, *J.*
975 *Geophys. Res. Atmos.*, *126*, e2020JD033617, doi:10.1029/2020JD033617.
976 Thompson, D. W. J., and S. Solomon (2002), Interpretation of recent Southern Hemisphere
977 climate change, *Science (80-.).*, *296*, 895–899.
978 Trenberth, K. E., A. Dai, R. M. Rasmussen, and D. B. Parsons (2003), The changing character
979 of precipitation, *Bull. Am. Meteorol. Soc.*, *84*(9), 1205–1217, doi:10.1175/BAMS-84-9-
980 1205.
981 Westra, S., H. J. Fowler, J. P. Evans, L. V Alexander, P. Berg, F. Johnson, E. J. Kendon, G.
982 Lenderink, and N. M. Roberts (2014), Reviews of Geophysics, *Rev. Geophys.*, *52*, 522–
983 555, doi:10.1002/2014RG000464.
984 Woollings, T., D. Barriopedro, J. Methven, S. W. Son, O. Martius, B. Harvey, J. Sillmann, A.
985 R. Lupo, and S. Seneviratne (2018), Blocking and its Response to Climate Change, *Curr.*
986 *Clim. Chang. Reports*, *4*(3), 287–300, doi:10.1007/s40641-018-0108-z.
987 Zhang, Z., F. M. Ralph, and M. Zheng (2019), The Relationship Between Extratropical Cyclone
988 Strength and Atmospheric River Intensity and Position, *Geophys. Res. Lett.*, *46*(3), 1814–
989 1823, doi:10.1029/2018GL079071.
990 Zheng, F., J. Li, R. T. Clark, and H. C. Nnamchi (2013), Simulation and projection of the
991 Southern Hemisphere annular mode in CMIP5 models, *J. Clim.*, *26*(24), 9860–9879,
992 doi:10.1175/JCLI-D-13-00204.1.
993 Zhu, Y., and R. E. Newell (1994), Atmospheric rivers and bombs, *Geophys. Res. Lett.*, *21*(18),
994 1999–2002, doi:10.1029/94GL01710.
995
996

Figures & Tables

	Low (Trough)			High (Ridge)			Gradient (Trough and Ridge)			
	Lat	**Lon**	**Min$_{Z'}$**	**Lat**	**Lon**	**Max$_{Z'}$**	**Diff$_{Lat}$**	**Diff$_{Lon}$**	**Diff$_{Z'}$**	**Grad**
T (Trough)	x	x	x							
SW (Southwesterly)	x	x	x							
TNW (Trough Northwesterly)	x	x	x	x	x	x	x	x	x	x
TSW (Trough Southwesterly)	x	x	x							
H (High)				x	x	x				
HNW (High to the Northwest)	x	x	x	x	x	x	x	x	x	x
W (Westerly)	x	x	x	x	x	x	x	x	x	x
HSE (High to the Southeast)				x	x	x				
HE (High to the East)	x	x	x	x	x	x	x	x	x	x
NE (Northeasterly)	x	x	x	x	x	x	x	x	x	x
HW (High to the West)	x	x	x	x	x	x	x	x	x	x
R (Ridge)	x	x	x	x	x	x	x	x	x	x

Table 1. Overview of the internal descriptors used for each of the 12 WTs seen in Fig. 1 (in rows), with their usual abbreviations and their long names after Ackerley et al., 2011 and Cullen et al., 2019. “Low” columns are for troughs, “High” columns for ridges, and “Gradient” columns for weather types showing both troughs and ridges. Descriptors depict the spatial coordinates (Lat, Lon) and intensities (MinZ’, MaxZ’) of the corresponding atmospheric centres of action, and for gradient types, their differences (DiffLat, DiffLon, DiffZ’). Grad corresponds to the geopotential height gradient between both centers of action (DiffZ’ / distance separating opposite centers of action).

For each AR timestep		Units
AR_IVTx	Vertically integrated vapor transport, zonal component	$kg.m^{-1}.s^{-1}$
AR_IVTy	Vertically integrated vapor transport, meridional component	
AR_IVTmag	Total vertically integrated vapor transport	
AR_IVT_direction	Angle of the vertically integrated vapor transport	°
For each AR event (sequence of consecutive timesteps)		
Max_IVT	Maximum value of vertically integrated vapor transport	$kg.m^{-1}.s^{-1}$
Max_IVTx	Maximum value of vertically integrated vapor transport, zonal component	
Max_IVTy	Maximum value of vertically integrated vapor transport, meridional component	
Max_direction	Angle of the maximum vertically integrated vapor transport	°
Duration	Duration of the AR sequence	h
Storm_total_IVT	Time integrated moisture transport	$kg.m^{-1}.s^{-1}$

Table 2. Overview of the AR metrics given by the Guan and Waliser (2019) AR detection algorithm that are analyzed in this work. The first category of metrics is given for each timestep associated with an AR event, while the second category is a statistics calculated over the whole duration (all timesteps included) of the AR event. Units are given by the third column.

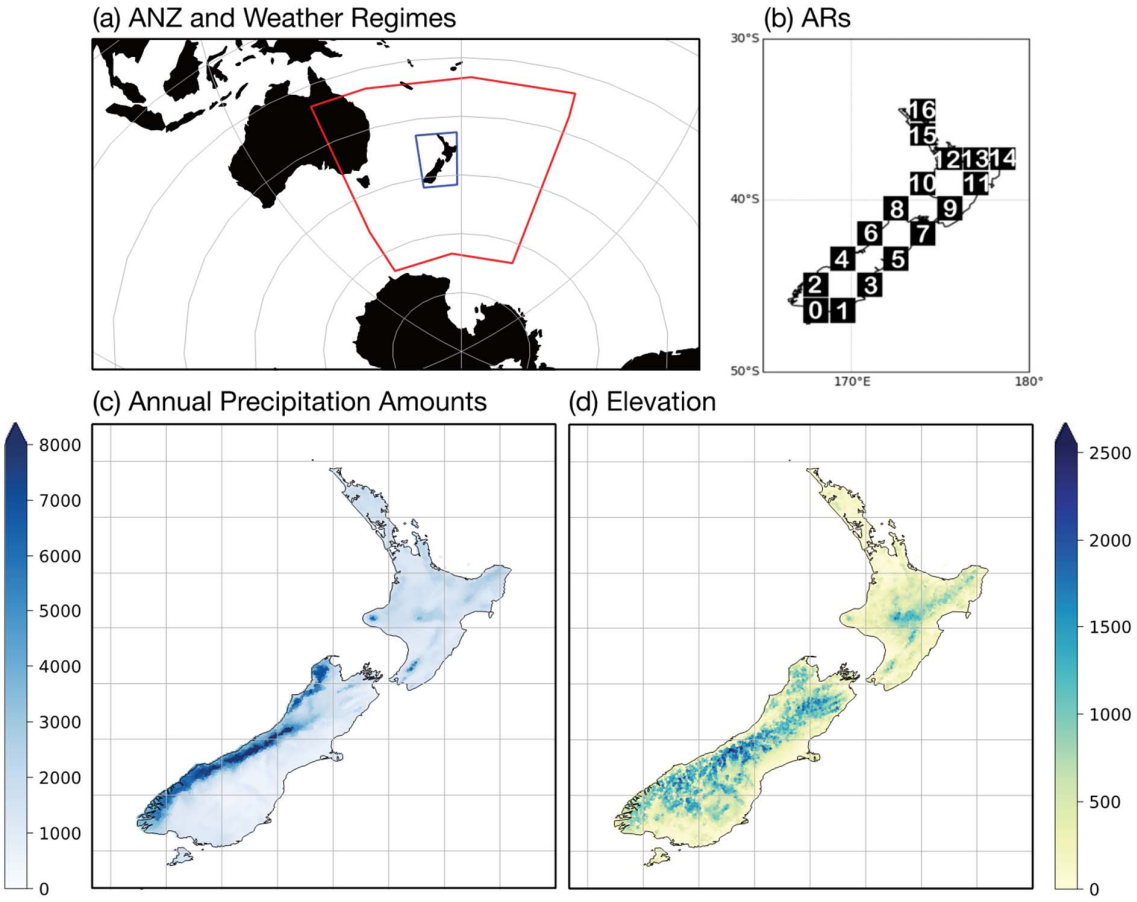

Figure 1. Domain locations, local climate and topography around ANZ. (a) Location of ANZ and domain boundaries used to analyze weather types and their atmospheric centers of action (in red), and local precipitation anomalies in ANZ (in blue). (b) Location and numbering of the 17 ERA-I grid-points used for AR detection. (c) Climatological mean annual precipitation amounts (mm) according to VCSN data, period 1979-2019. (d) Elevation (m above sea level).

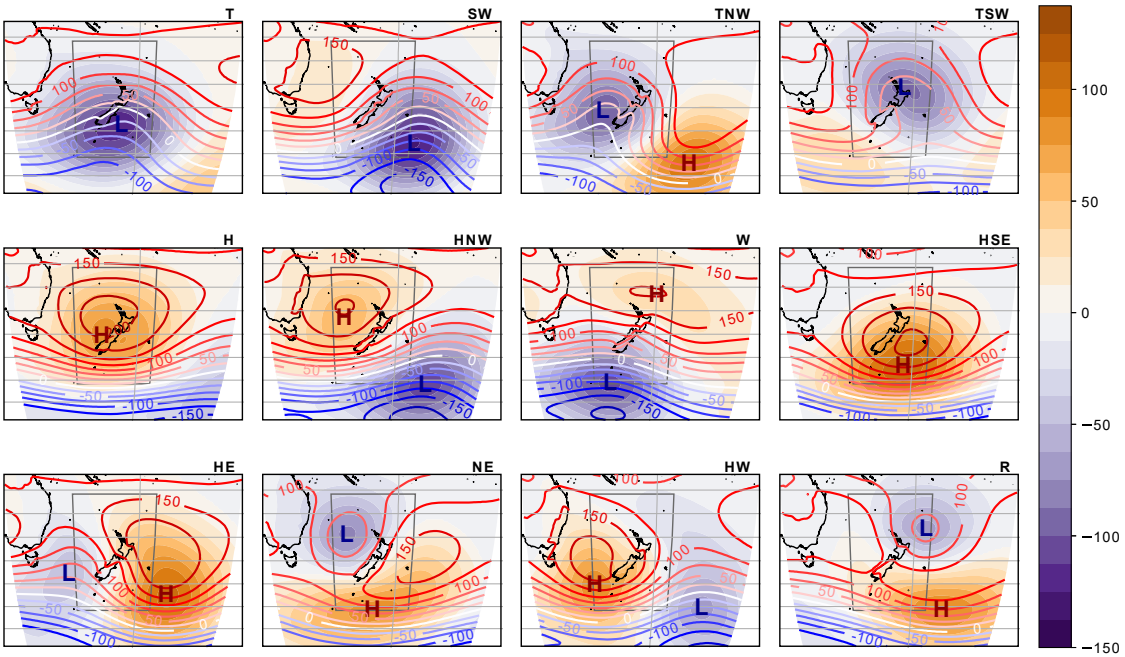

Figure 2. Geopotential height at 1000 hPa associated with the 12 weather types of Kidson (2000). Contours show composite mean Z1000 fields, colors show corresponding Z1000 anomalies. Geopotential heights are derived from ERA5 for the period 1979–2019. Only anomalies that are statistically different from the climatology according to a one-tailed t test at the 95% level are represented. The inner rectangle represents the original domain used by Kidson (2000). Letter H indicates local maximum Z1000 anomalies; L indicates local minimum Z1000 anomalies. ERA5 definition of WTs is used. Each WT is labeled with a descriptor that is used for referencing throughout the manuscript.

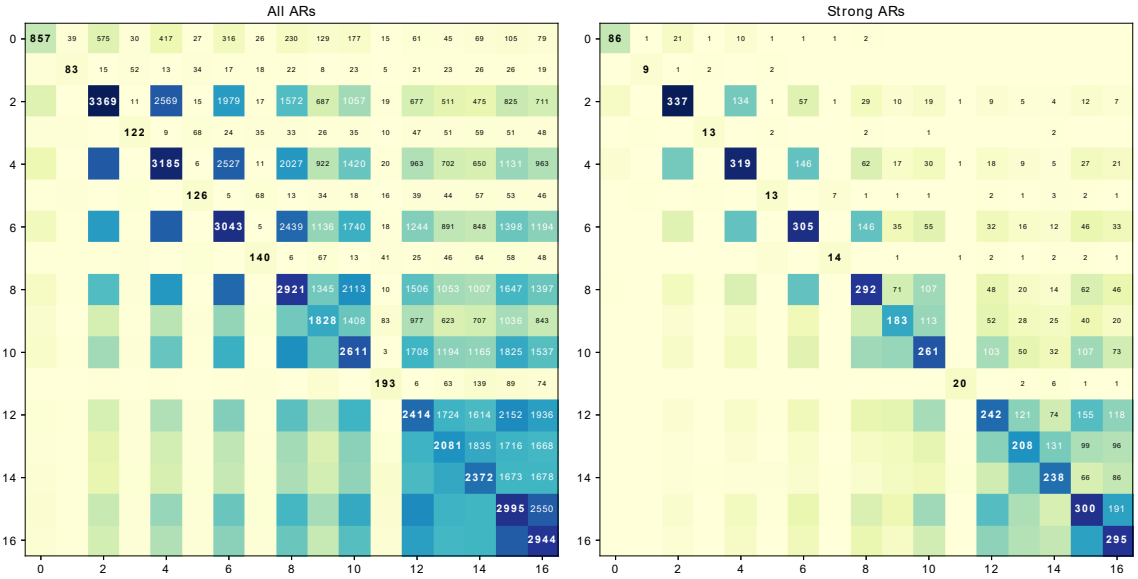

Figure 3. Co-occurrence of AR across grid-points (left all ARs reaching NZ; right: 10% strongest ARs according to the Max_IVT descriptor). Grid-points numbered as in Fig. 1b. Diagonal: number of days identified as ARs for each grid-point, period 1979-2019. Other cells: number of days identified as ARs co-occurring in the two corresponding grid-points.

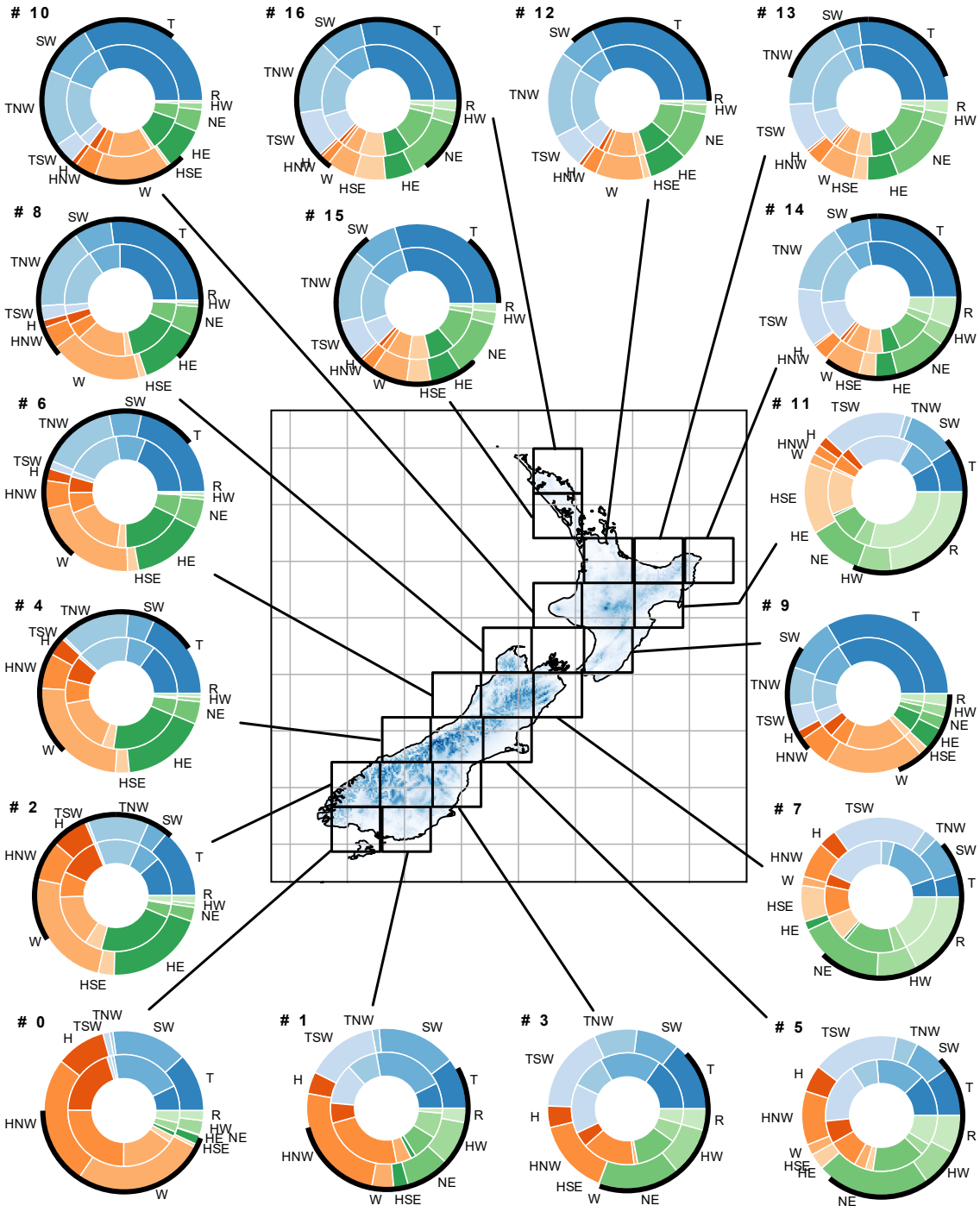

Figure 4. AR occurrence by Kidson type for each grid-point (as numbered in Fig. 1b), period 1979-2019. Outer pie plots: ERA5 redefinition of Kidson types; inner pie plot: original NCEP distribution. The black circle arcs out of the pie plots show the retained AR detection at each grid-point (landfalling ARs discarded when coming from the missing parts of the circles).

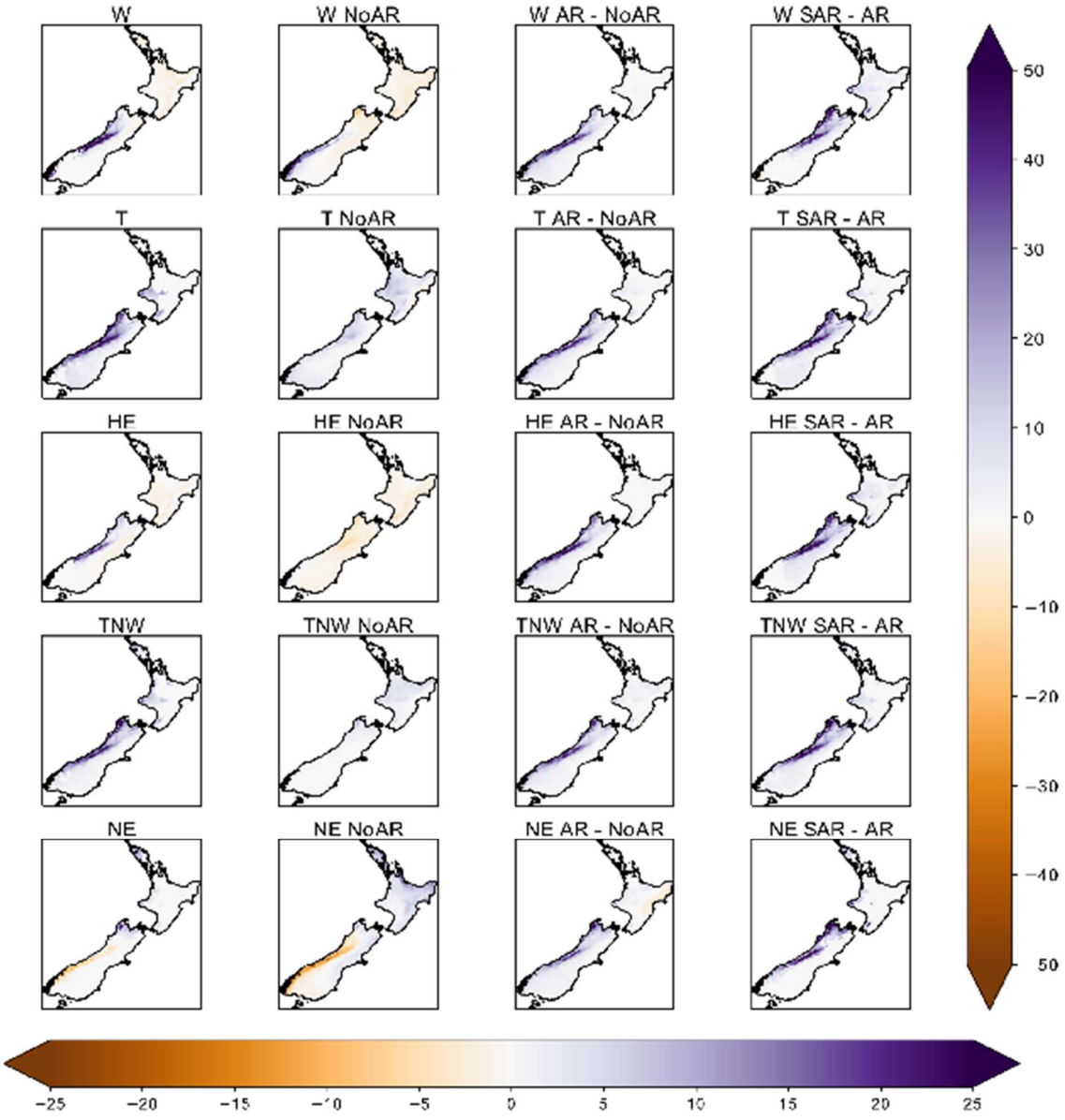

Figure 5. Daily precipitation anomalies (mm) associated with WTs when associated and not associated with ARs, g-p #6 (West Coast of the South Island). Composite precipitation anomalies (mm) during the 5 most favorable WTs (all days considered: 1st column) and during their occurrences not associated with ARs (2nd column), differences between NoAR days and moderate AR days (3rd column), and differences between strong AR days and moderate AR days (4th column). For the two first columns (lower colorbar), only significant anomalies against the climatology according to one-tailed t-tests modified by Welch (95% level) are displayed. For the third and fourth columns (right-hand colorbar), only significant differences according to two-tailed t-tests modified by Welch (95% level) are displayed. ERA5 redefinition of WTs is used.

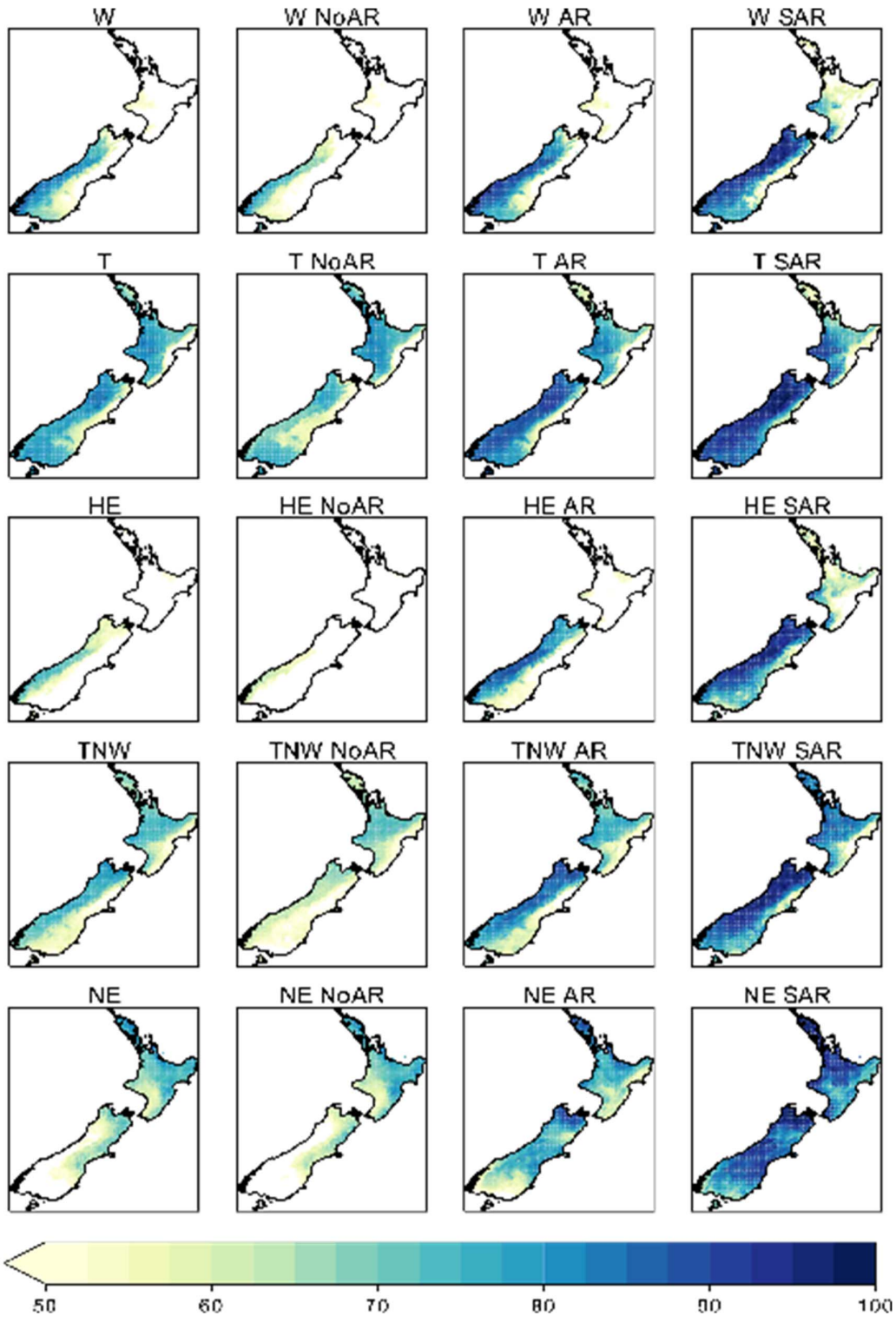

Figure 6. (a) Rank of daily precipitation anomalies associated with the 5 most favorable regimes, for NoAR, moderate AR and strong AR days. (a) Median and (b) 90th percentile of daily ranks for each WR and AR combination, for g-p #6 (West Coast of the South Island). Only rank values exceeding the 50th percentile (for a) and the 90th percentile (for b) are represented. ERA5 definition of WTs is used.

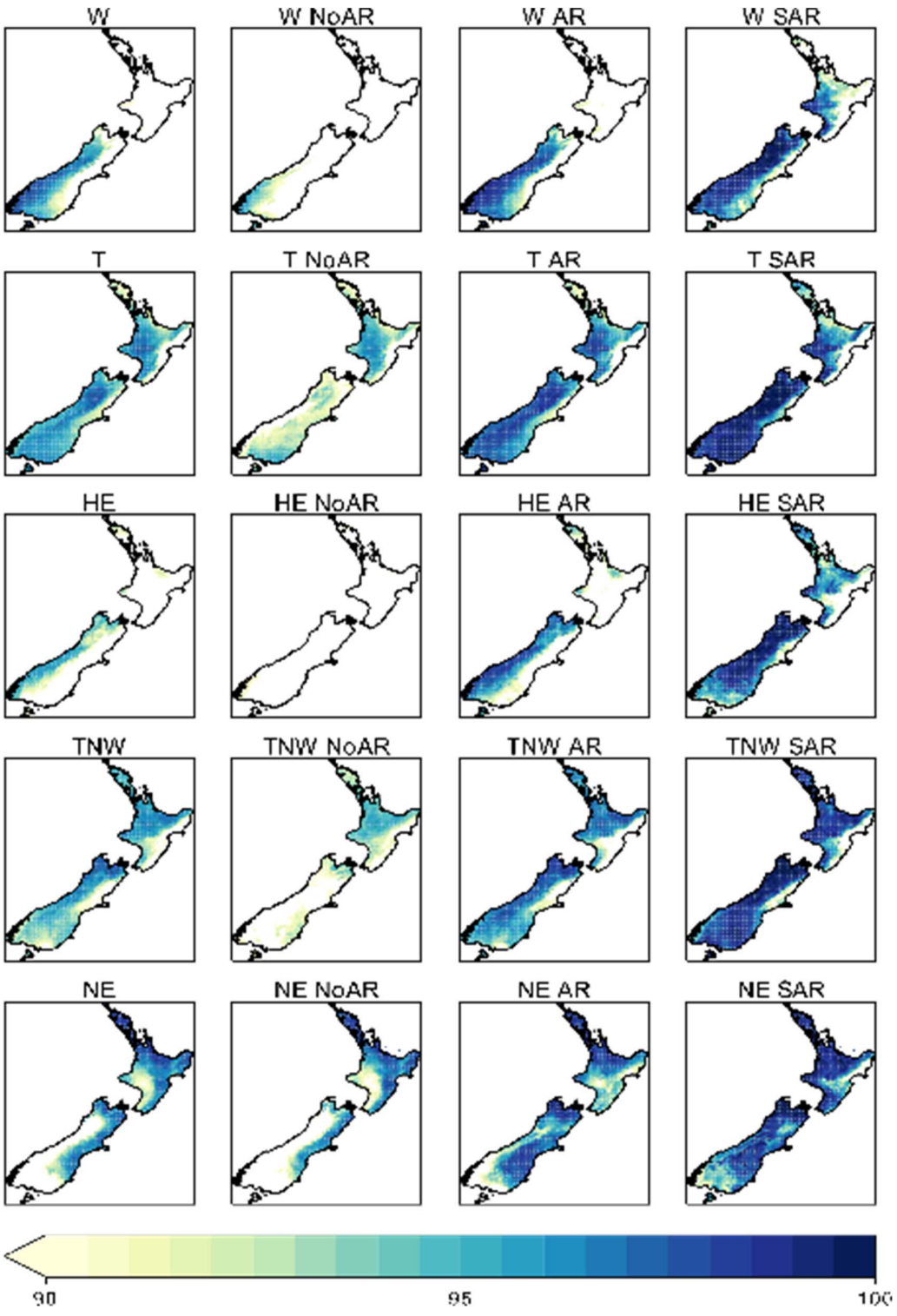

Fig. 6 (b: *continued*).

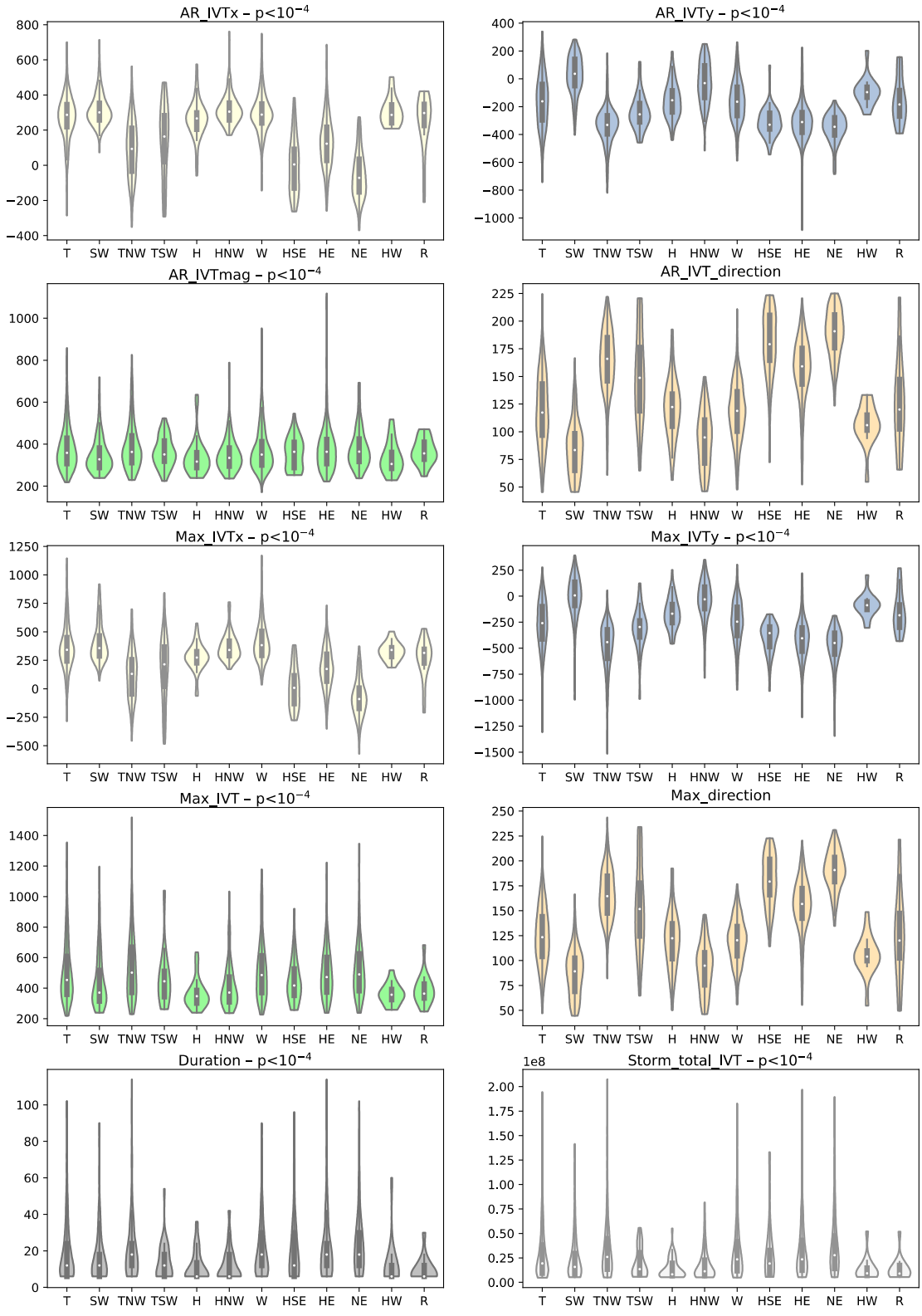
AR_IVTx – p<10⁻⁴
AR_IVTy – p<10⁻⁴
AR_IVTmag – p<10⁻⁴
AR_IVT_direction
Max_IVTx – p<10⁻⁴
Max_IVTy – p<10⁻⁴
Max_IVT – p<10⁻⁴
Max_direction
Duration – p<10⁻⁴
Storm_total_IVT – p<10⁻⁴
1e8
T SW TNW TSW H HNW W HSE HE NE HW R

←**Figure 7. Modulation of AR properties by the weather types** for grid-point #6 (West Coast of the South Island). Inner boxes: from 1st to 3rd quartiles (50% of the samples) with median value given by white circles. Whiskers show the range of the distributions, and violin plots represent smoothed observation densities. For quantitative values (all except IVT directions), labels indicate the estimated significance according to analyses of variance (ANOVAs). ERA5 definition of WTs is used.

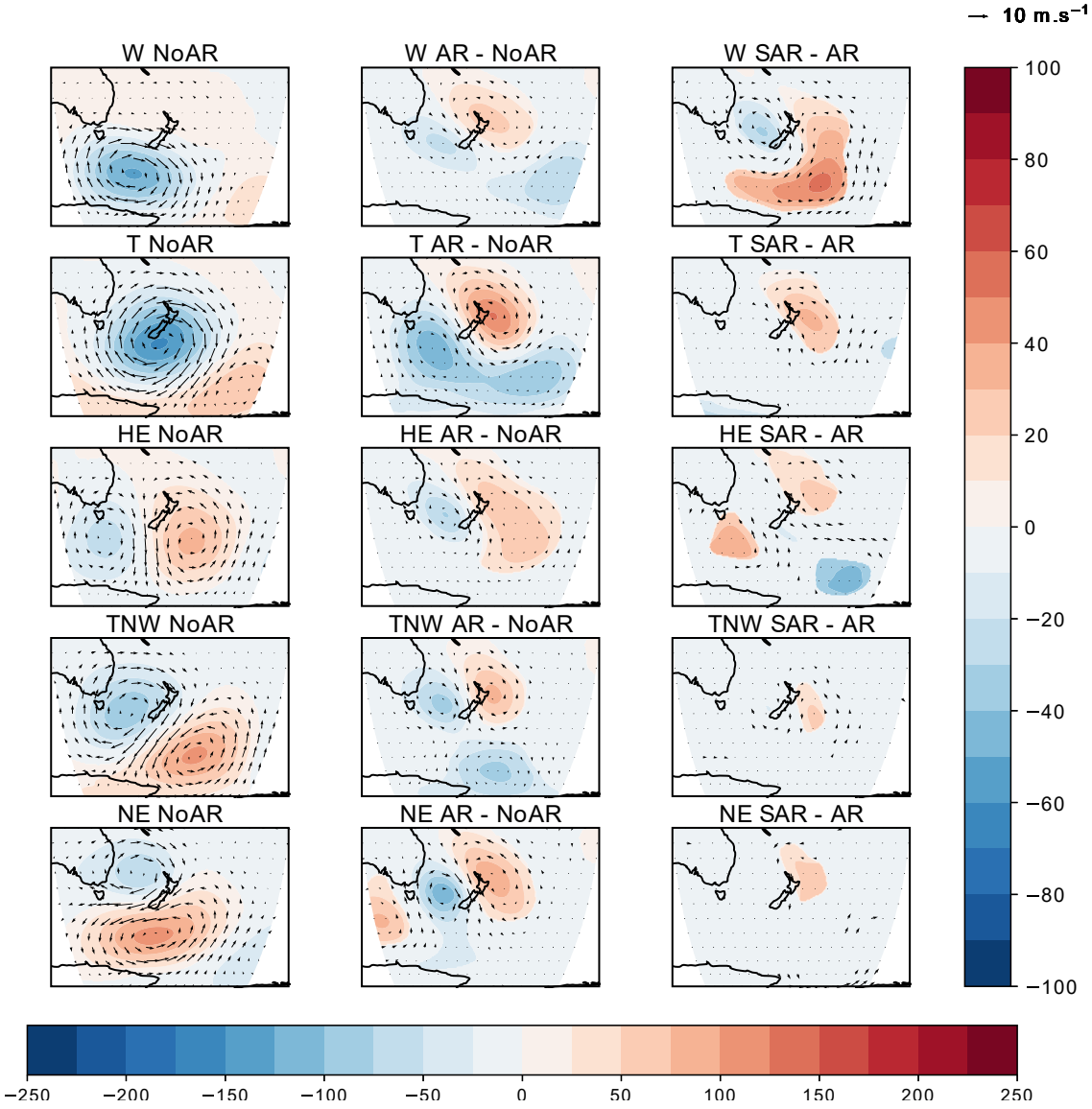

Figure 8. (a) Differences in synoptic conditions between WTs associated and not associated with ARs in grid-point #6 (West Coast of the South Island) and (a) for the ERA5 redefinition of WTs, and (b) for the original NCEP/NCAR definition of the WTs. Composite mean geopotential height anomalies at 700hPa (colors: m) and 700hPa horizontal wind anomalies (vectors: $m.s^{-1}$) anomalies during the 5 most favorable WTs (a: ERA5 redefinition of WTs; b: NCEP/NCAR original definition of the WTs). In each figure: left column, most favorable WTs when not associated with ARs. Middle column: difference between NoAR and moderate AR occurrences of the same WTs. Right: difference between strong ARs (SAR: top 10% IVT) and moderate ARs. For the two first columns (lower colorbar), only significant anomalies according to one-tailed t-tests modified by Welch (95% level) are displayed. For the third column (right-hand colorbar), only significant differences according to two-tailed t-tests modified by Welch (95% level) are displayed.

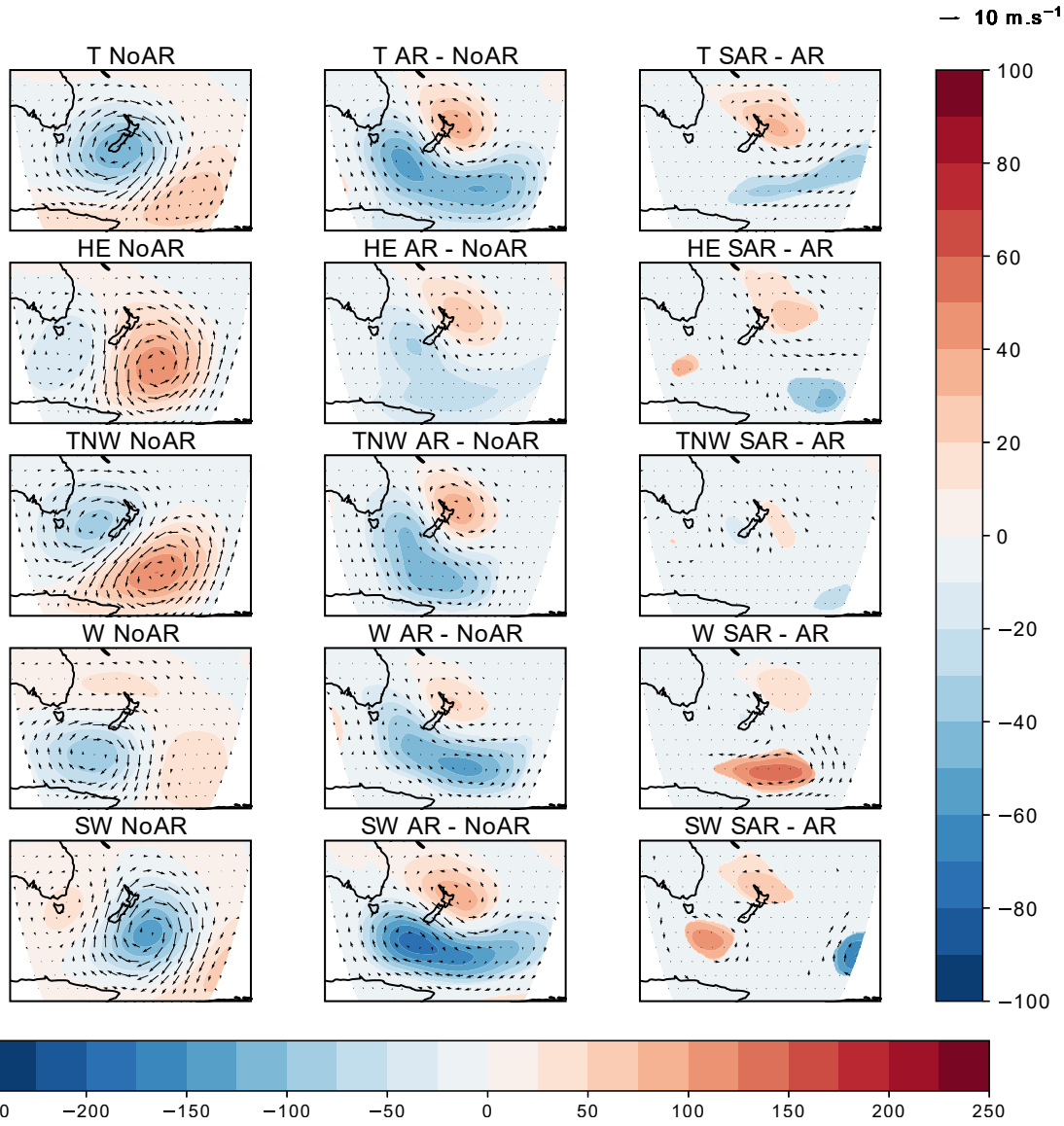

Fig. 8 (b: *continued*).

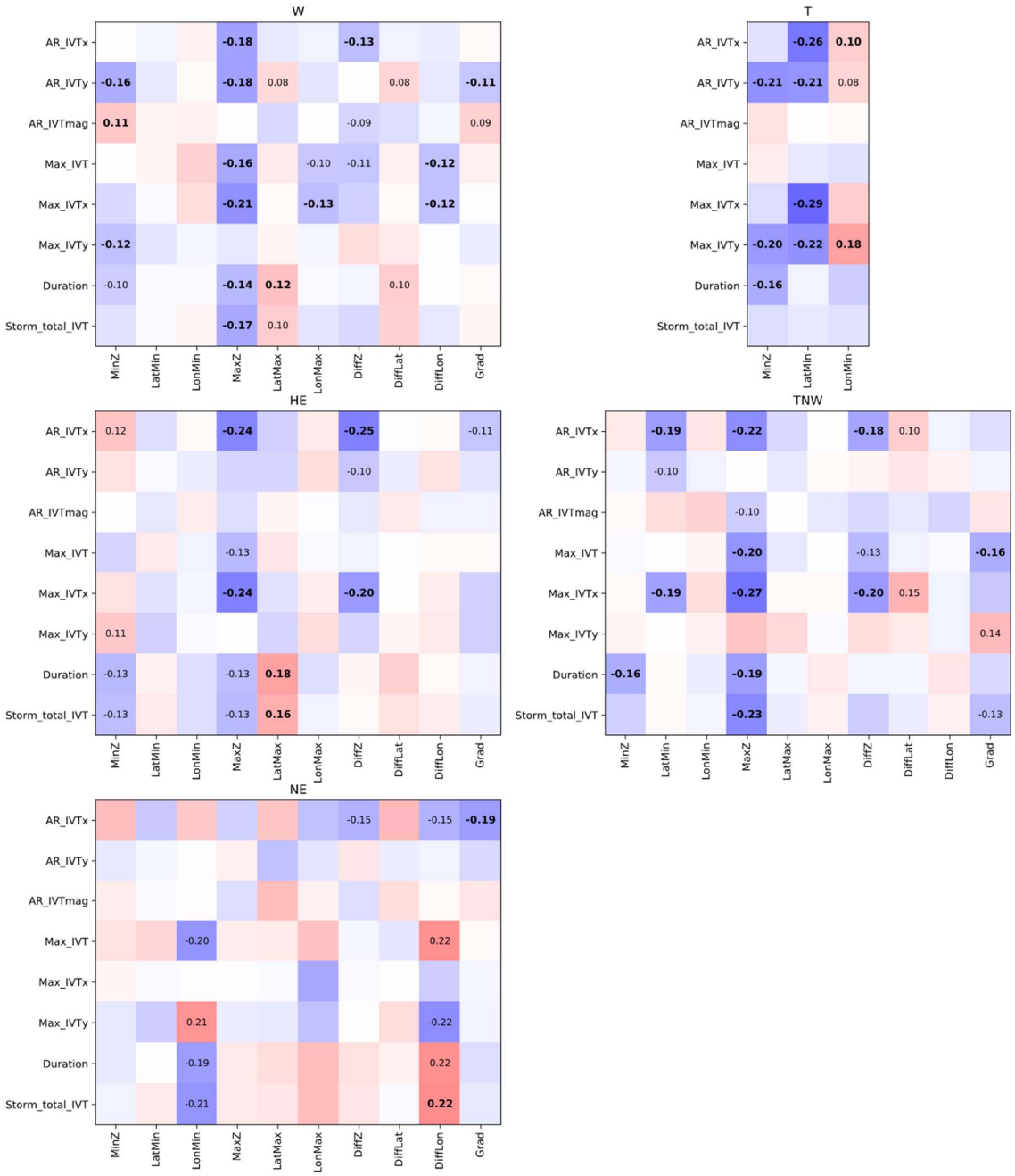

Figure 9. (a) Daily correlations between KT descriptors and AR features for the 5 most favorable KTs according to ERA5 definition of WTs for grid-point #6 (West Coast of the South Island) and (a) for the ERA5 redefinition of WTs, and (b) for the original NCEP/NCAR definition of the WTs. Correlations not significant at 95% omitted, correlations above the 99% threshold in bold.

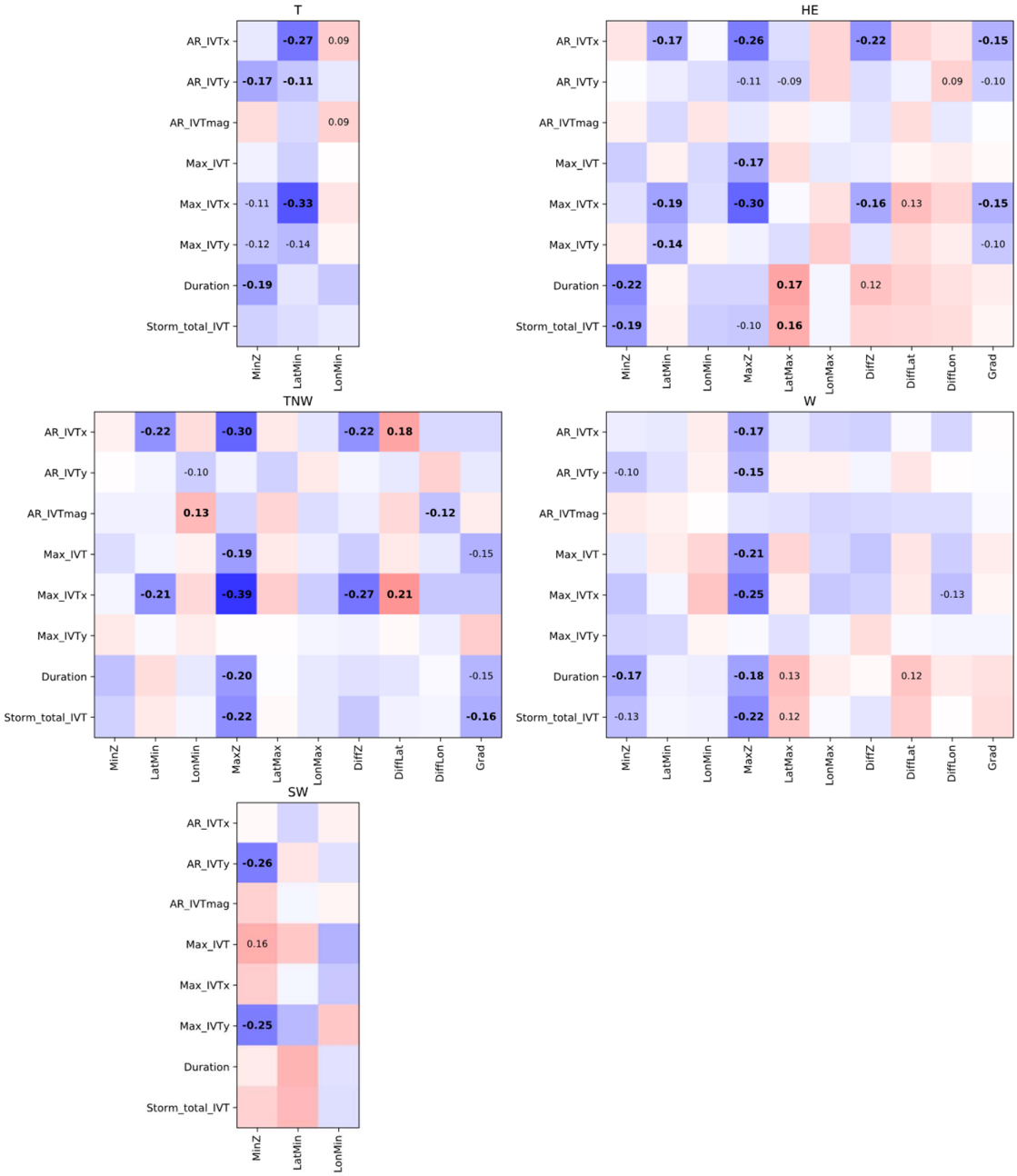

Fig. 9 (b: *continued*).

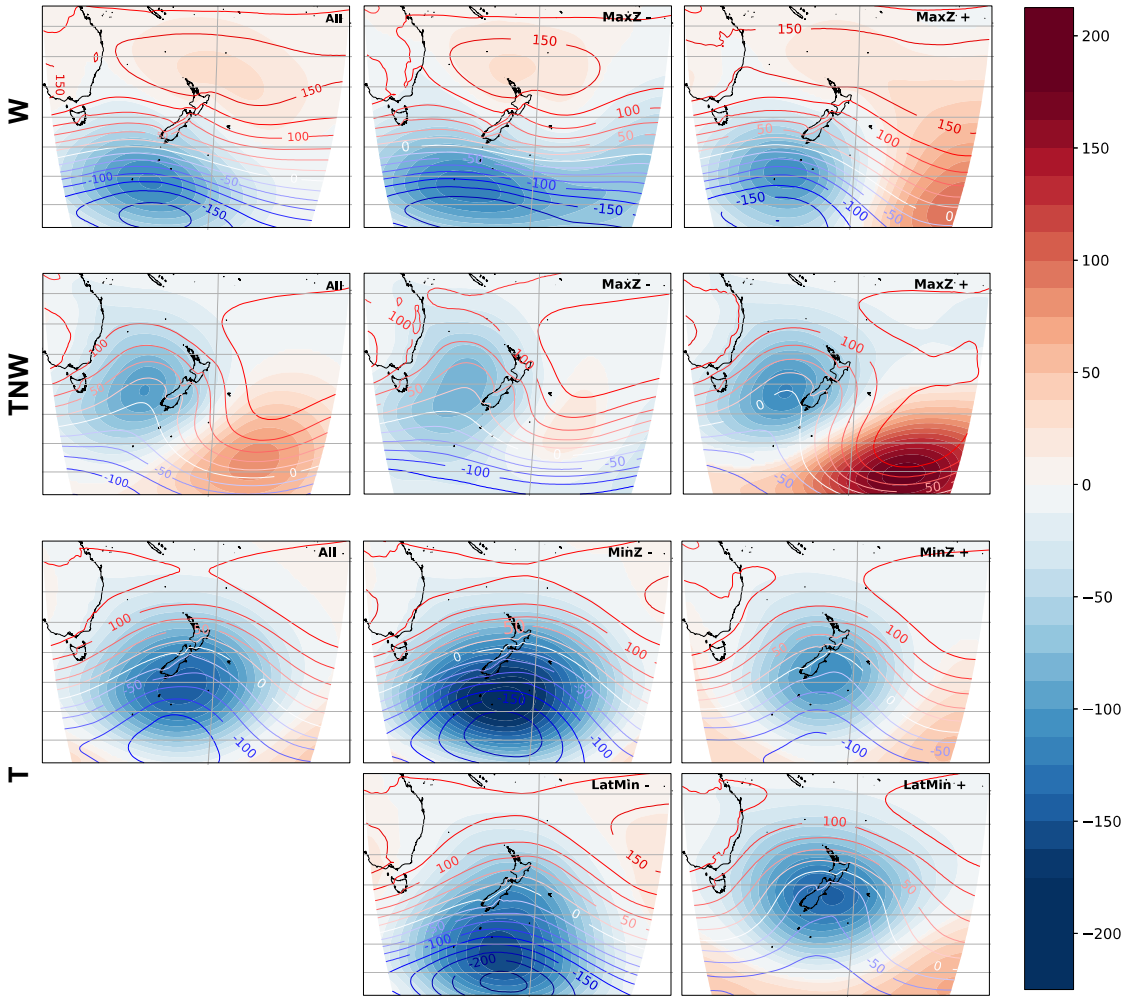

Figure 10. Composite mean Z1000 fields associated with the opposite phases of WT descriptors for WTs W, TNW and T controlling AR differences in grid-point #6 (West Coast of the South Island). The left-hand column shows the composite mean anomaly pattern of Z1000 raw fields (contours) and corresponding anomalies (colors) during all days ascribed to the corresponding WTs. The two remaining columns show the sub-samples formed by the opposite phases of the WT descriptor labeled in the figure. Opposite phases of each descriptor of each WT are extracted using their 20th and 80th percentiles. In all maps, only significant anomalies according to one-tailed t-tests modified by Welch (95% level) are displayed.

Figure 1.

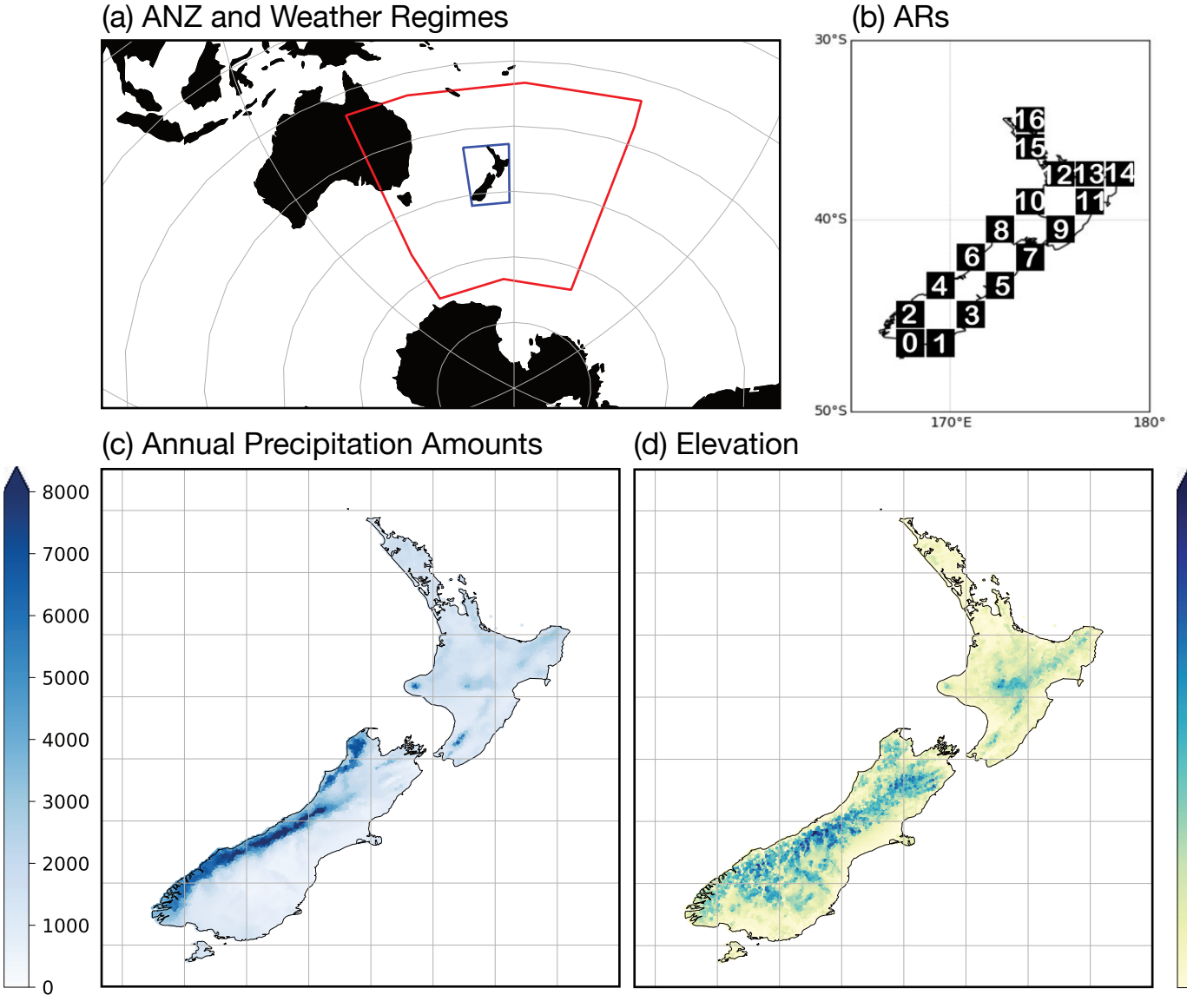
(a) ANZ and Weather Regimes
(b) ARs
30°S
40°S
50°S
170°E
180°
16
15
12
13
14
10
11
8
9
6
7
4
5
2
3
0
1
(c) Annual Precipitation Amounts
8000
7000
6000
5000
4000
3000
2000
1000
0
(d) Elevation
2500
2000
1500
1000
500
0

Figure 2.

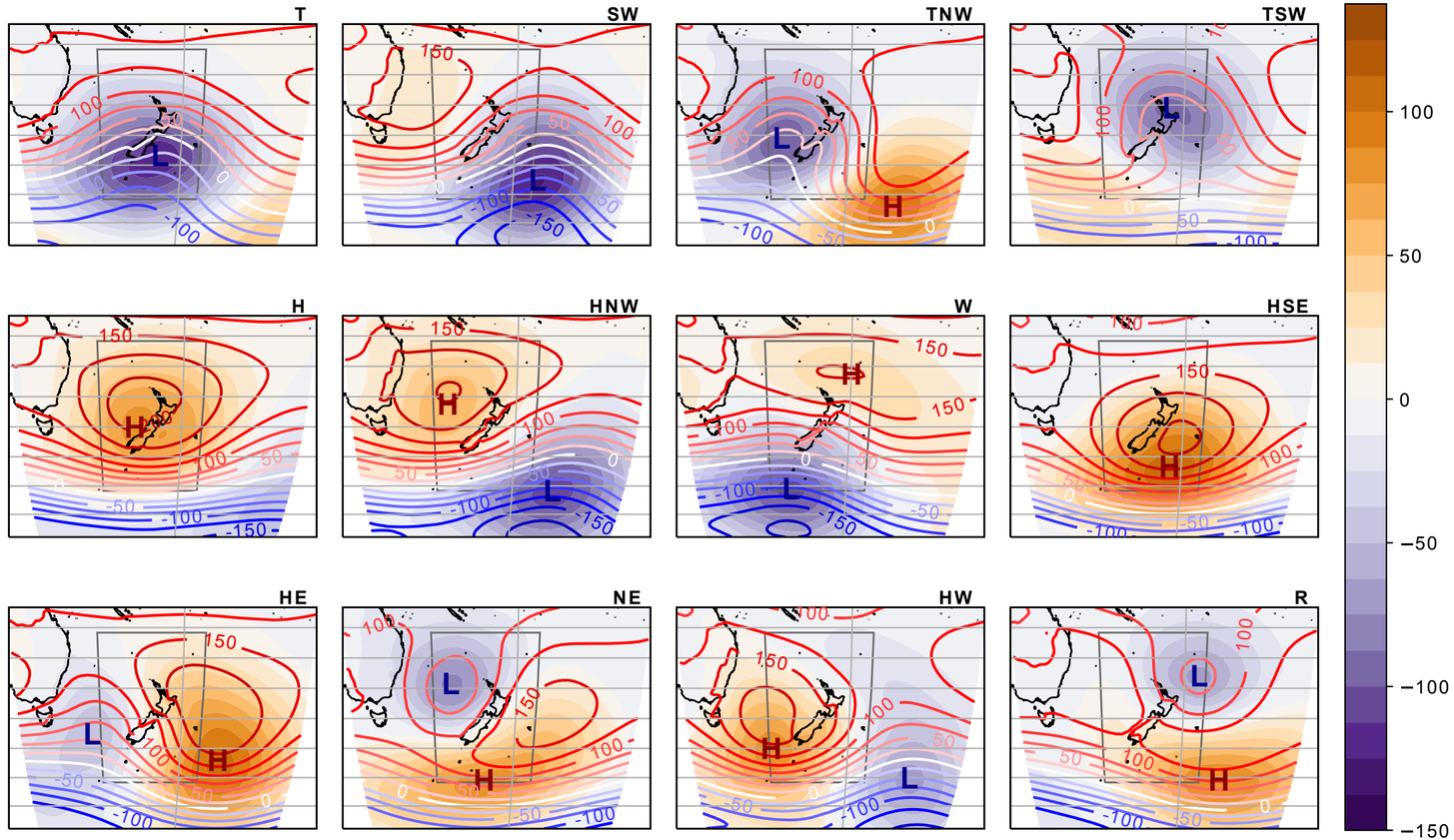
T
SW
TNW
TSW
H
HNW
W
HSE
HE
NE
HW
R
100
50
0
−50
−100
−150

Figure 3.

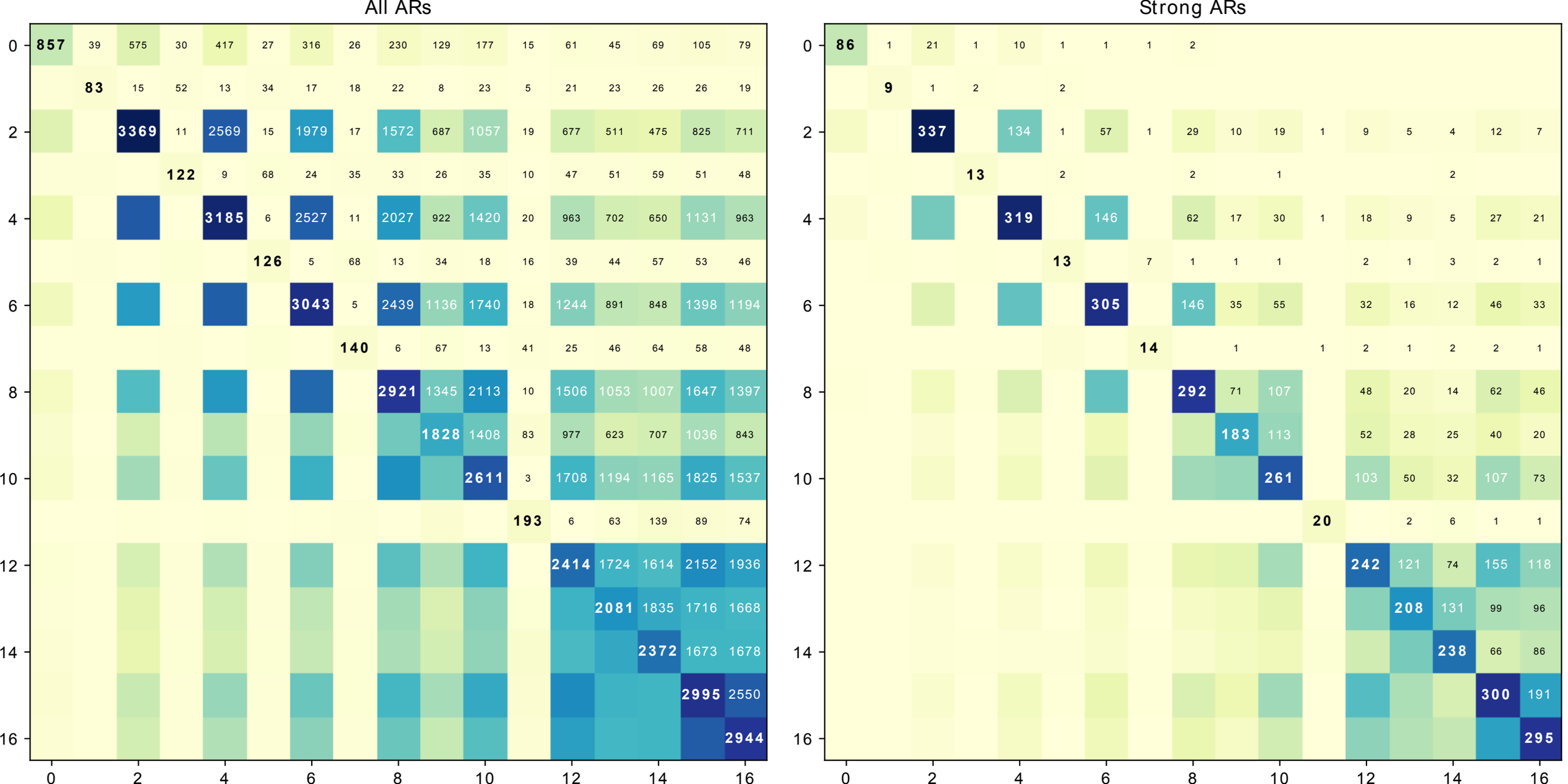
All ARs
Strong ARs
0
2
4
6
8
10
12
14
16
857 39 575 30 417 27 316 26 230 129 177 15 61 45 69 105 79
83 15 52 13 34 17 18 22 8 23 5 21 23 26 26 19
3369 11 2569 15 1979 17 1572 687 1057 19 677 511 475 825 711
122 9 68 24 35 33 26 35 10 47 51 59 51 48
3185 6 2527 11 2027 922 1420 20 963 702 650 1131 963
126 5 68 13 34 18 16 39 44 57 53 46
3043 5 2439 1136 1740 18 1244 891 848 1398 1194
140 6 67 13 41 25 46 64 58 48
2921 1345 2113 10 1506 1053 1007 1647 1397
1828 1408 83 977 623 707 1036 843
2611 3 1708 1194 1165 1825 1537
193 6 63 139 89 74
2414 1724 1614 2152 1936
2081 1835 1716 1668
2372 1673 1678
2995 2550
2944
86 1 21 1 10 1 1 1 2
9 1 2 2
337 134 1 57 1 29 10 19 1 9 5 4 12 7
13 2 2 1 2
319 146 62 17 30 1 18 9 5 27 21
13 7 1 1 1 2 1 3 2 1
305 146 35 55 32 16 12 46 33
14 1 1 2 1 2 2 1
292 71 107 48 20 14 62 46
183 113 52 28 25 40 20
261 103 50 32 107 73
20 2 6 1 1
242 121 74 155 118
208 131 99 96
238 66 86
300 191
295

Figure 4.

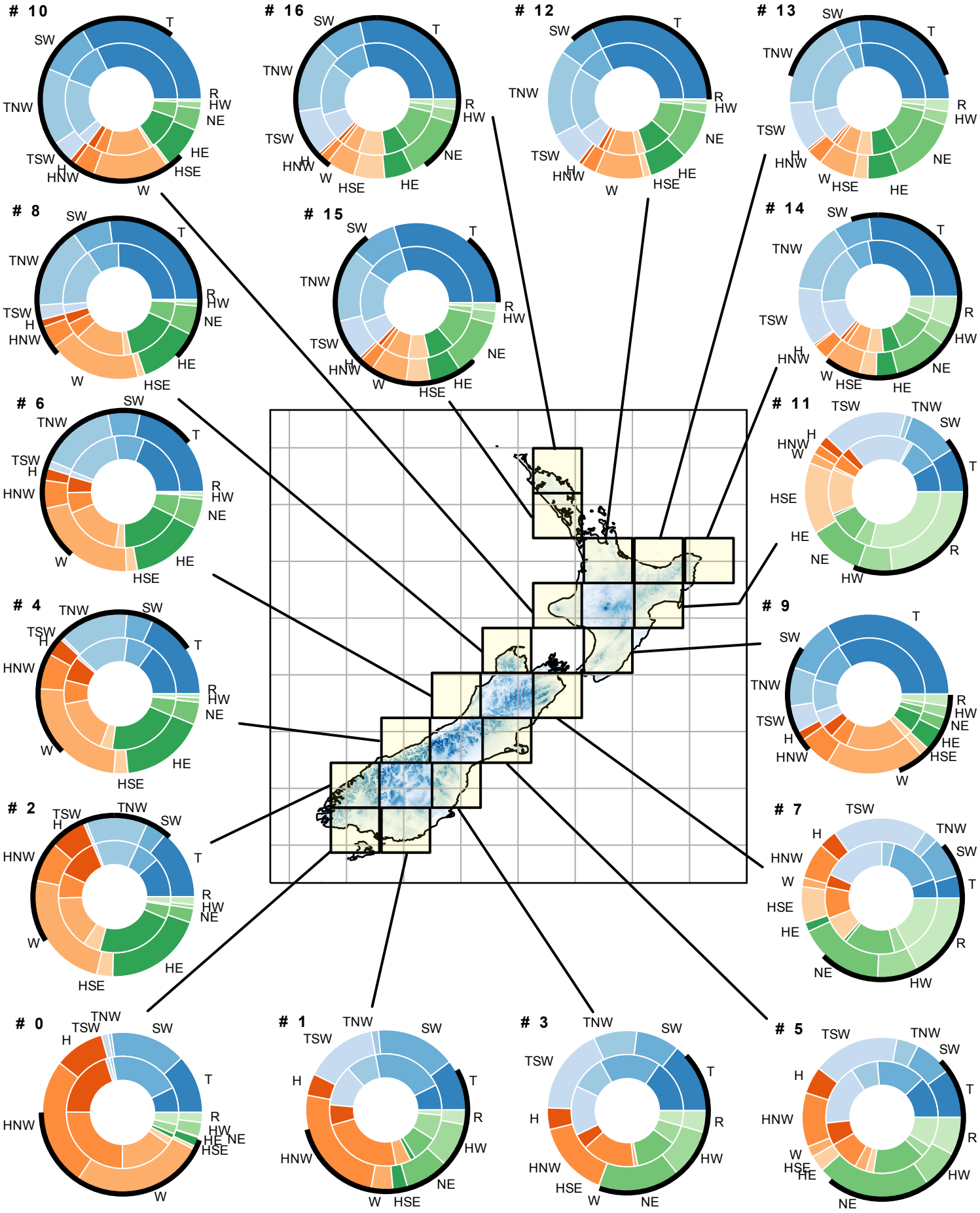
10
16
12
13
8
15
14
6
11
4
9
2
7
0
1
3
5
T
SW
TNW
TSW
H
HNW
W
HSE
HE
NE
HW
R

Figure 5.

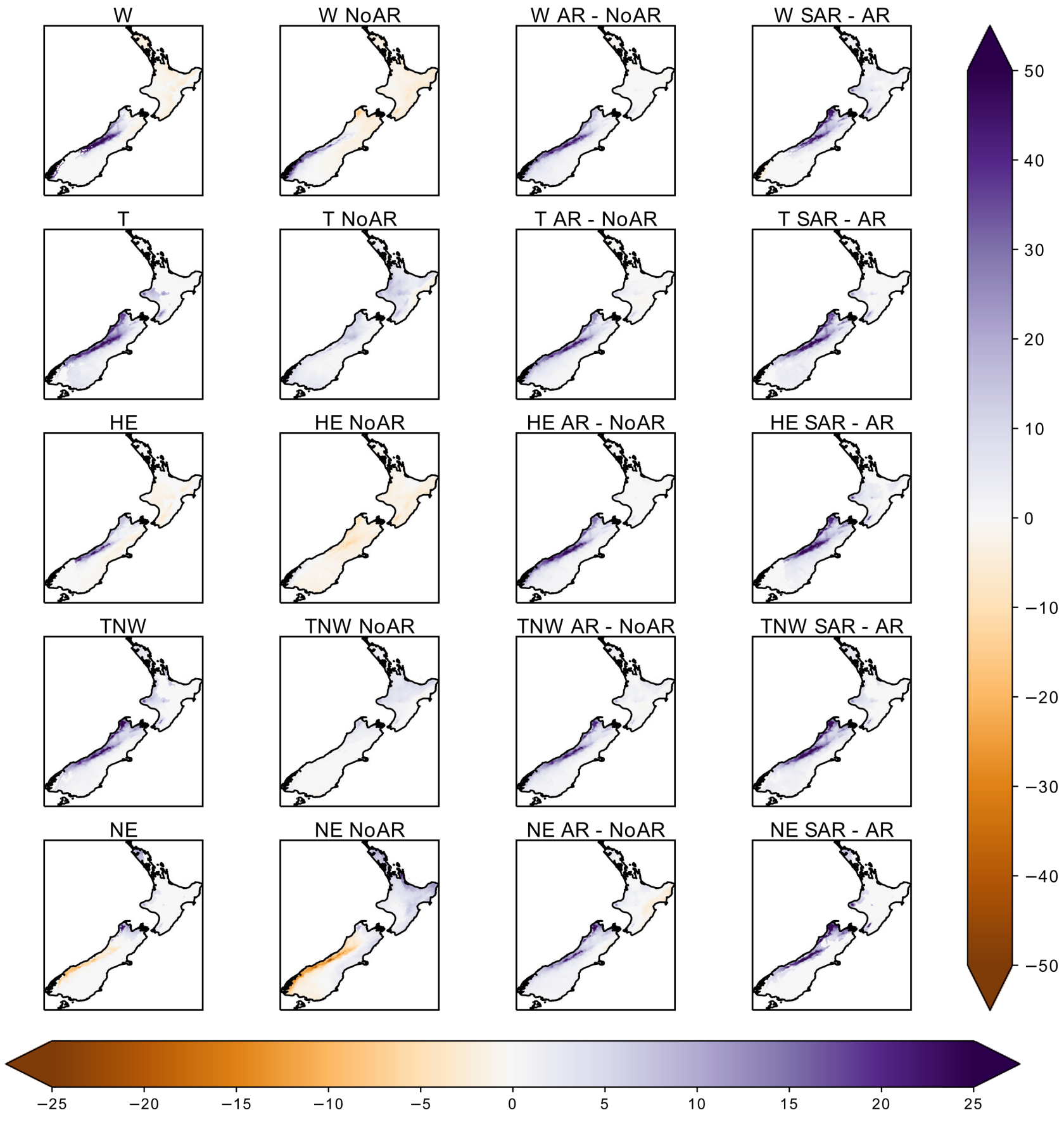
W
W NoAR
W AR - NoAR
W SAR - AR
T
T NoAR
T AR - NoAR
T SAR - AR
HE
HE NoAR
HE AR - NoAR
HE SAR - AR
TNW
TNW NoAR
TNW AR - NoAR
TNW SAR - AR
NE
NE NoAR
NE AR - NoAR
NE SAR - AR
50
40
30
20
10
0
−10
−20
−30
−40
−50
−25
−20
−15
−10
−5
0
5
10
15
20
25

Figure 6a.

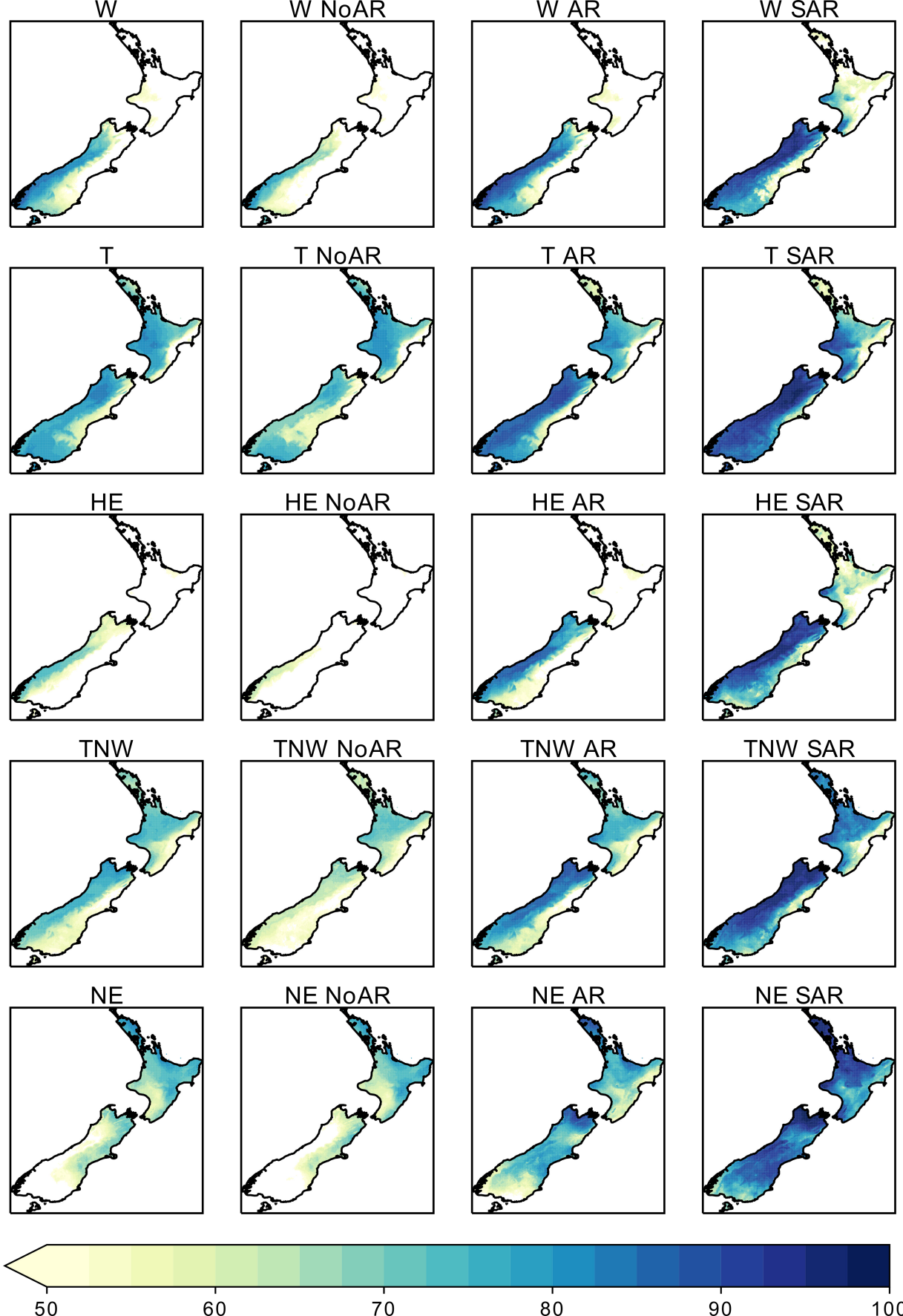
W
W NoAR
W AR
W SAR
T
T NoAR
T AR
T SAR
HE
HE NoAR
HE AR
HE SAR
TNW
TNW NoAR
TNW AR
TNW SAR
NE
NE NoAR
NE AR
NE SAR
50
60
70
80
90
100

Figure 6b.

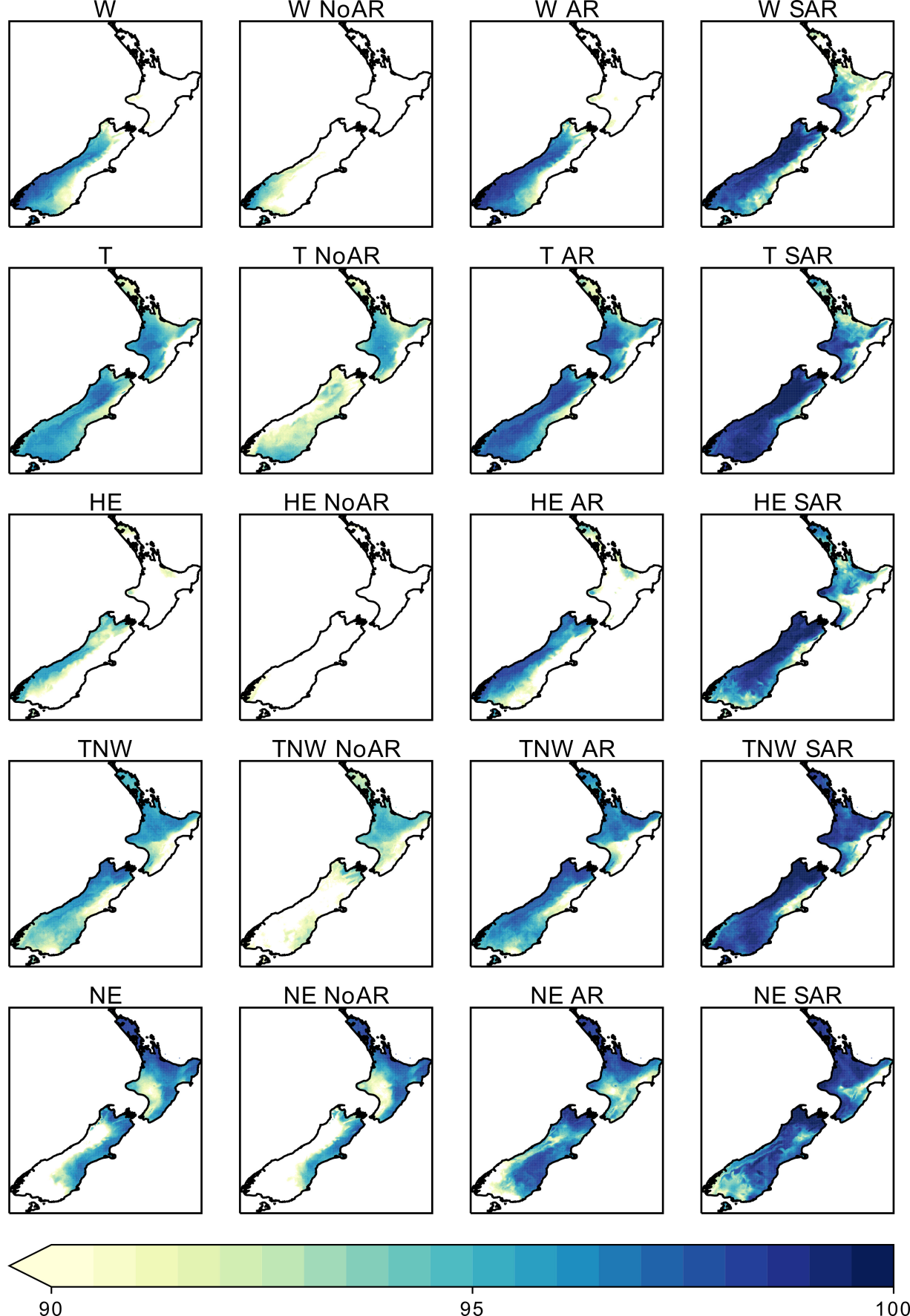
W
W NoAR
W AR
W SAR
T
T NoAR
T AR
T SAR
HE
HE NoAR
HE AR
HE SAR
TNW
TNW NoAR
TNW AR
TNW SAR
NE
NE NoAR
NE AR
NE SAR
90
95
100

Figure 7.

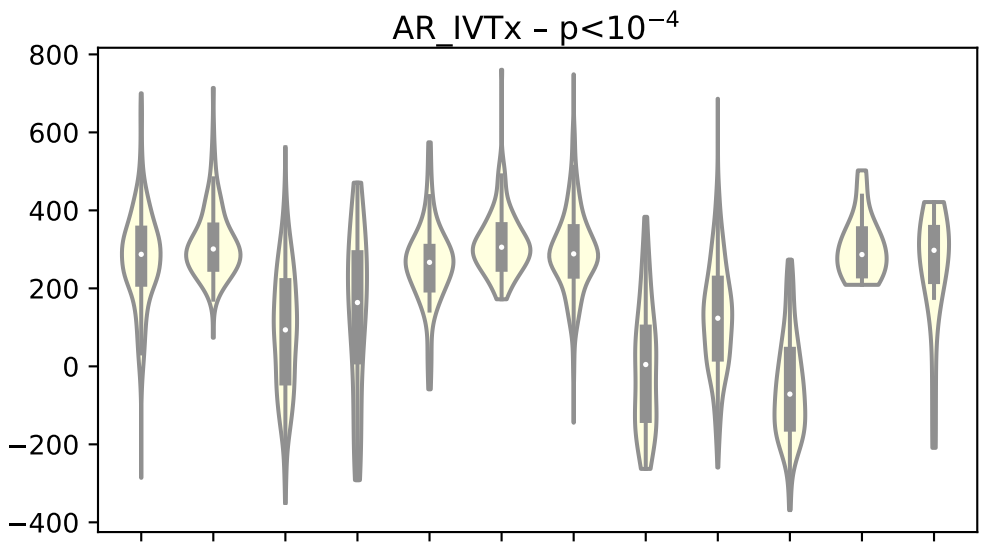
AR_IVTx – p<10^{-4}
800
600
400
200
0
−200
−400
T SW TNW TSW H HNW W HSE HE NE HW R

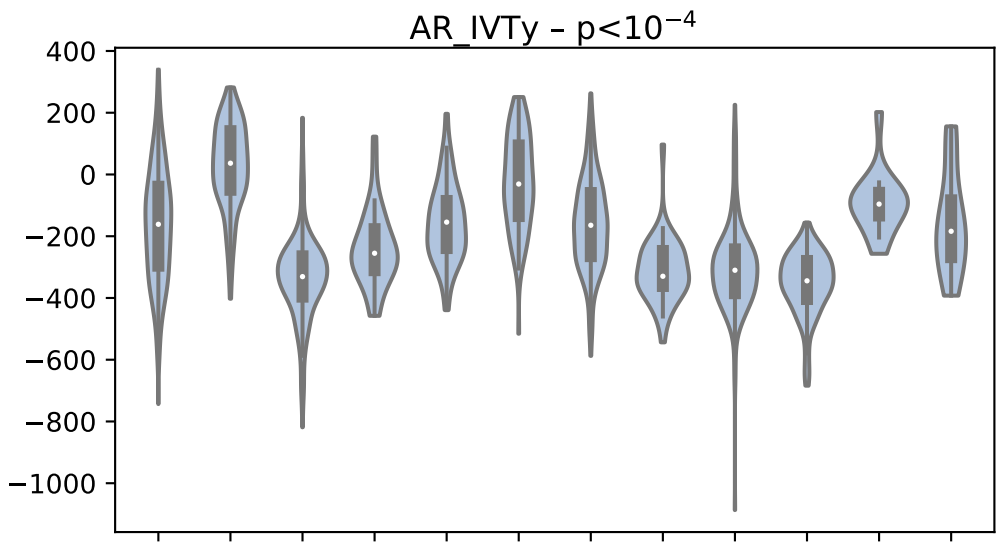
AR_IVTy – p<10^{-4}
400
200
0
−200
−400
−600
−800
−1000
T SW TNW TSW H HNW W HSE HE NE HW R

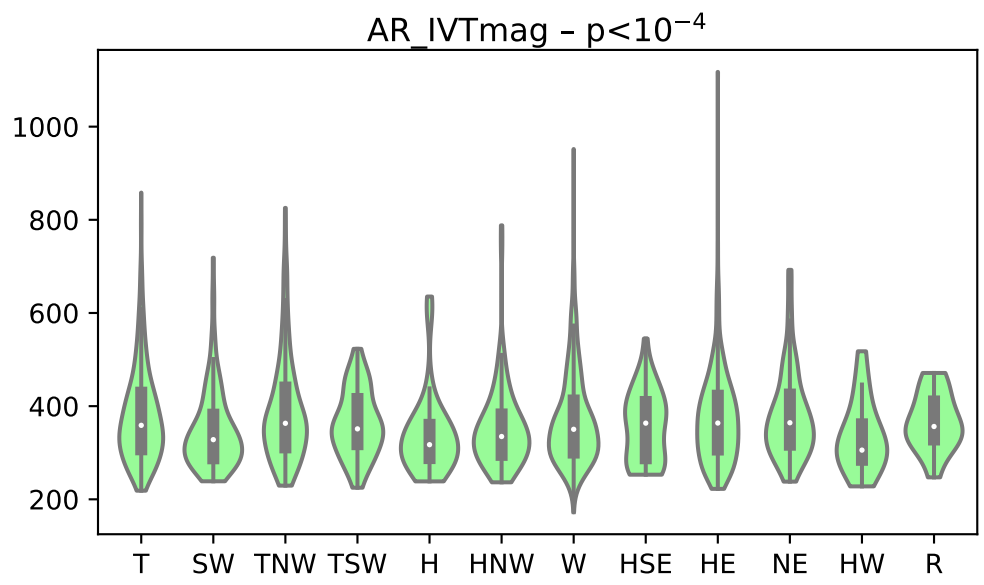
AR_IVTmag – p<10^{-4}
1000
800
600
400
200
T SW TNW TSW H HNW W HSE HE NE HW R

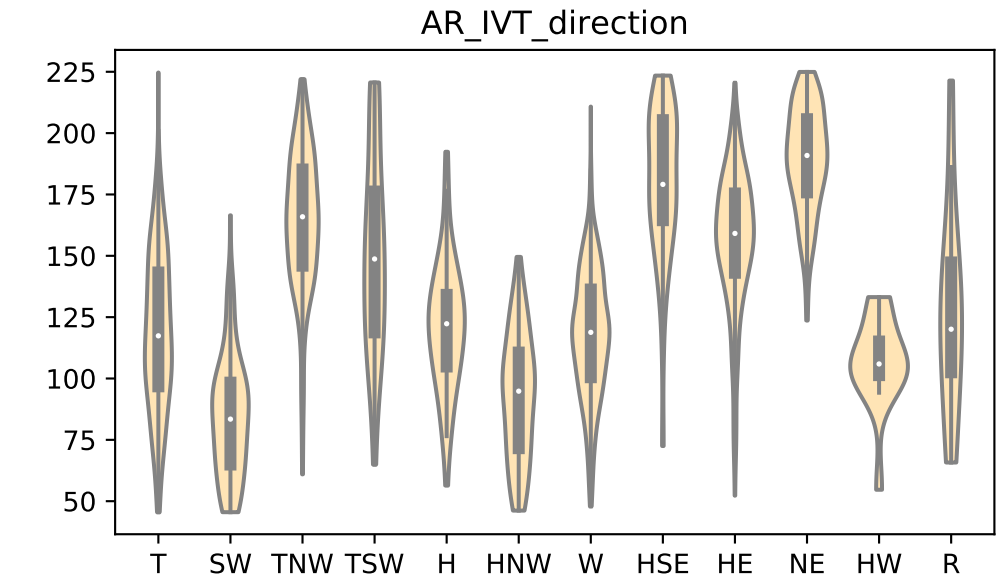
AR_IVT_direction
225
200
175
150
125
100
75
50
T SW TNW TSW H HNW W HSE HE NE HW R

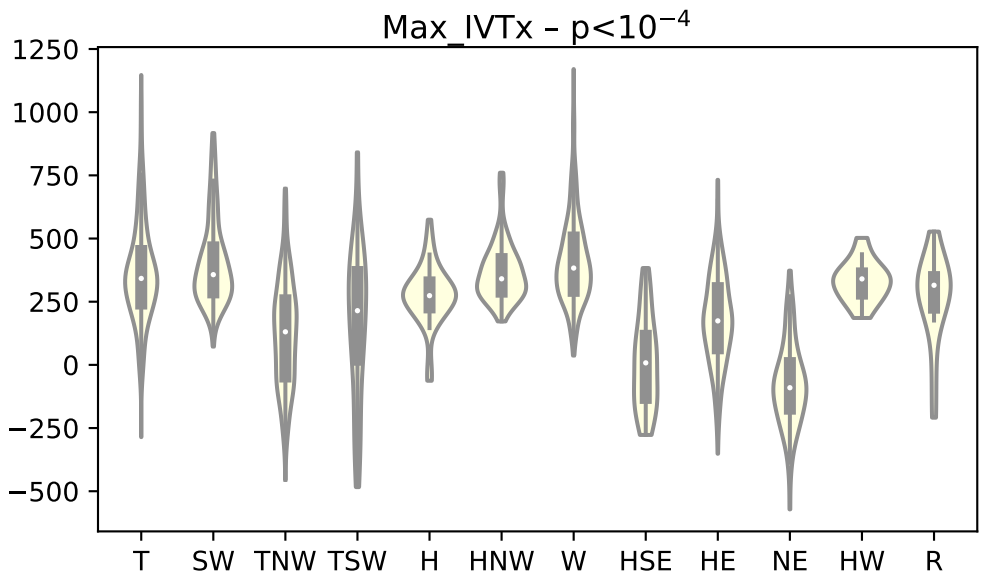
Max_IVTx – p<10^{-4}
1250
1000
750
500
250
0
−250
−500
T SW TNW TSW H HNW W HSE HE NE HW R

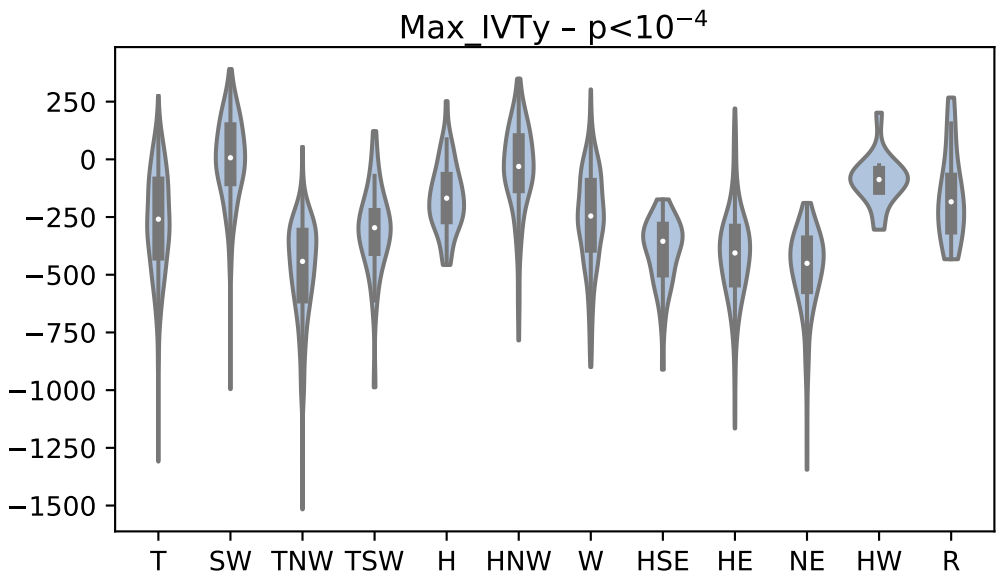
Max_IVTy – p<10^{-4}
250
0
−250
−500
−750
−1000
−1250
−1500
T SW TNW TSW H HNW W HSE HE NE HW R

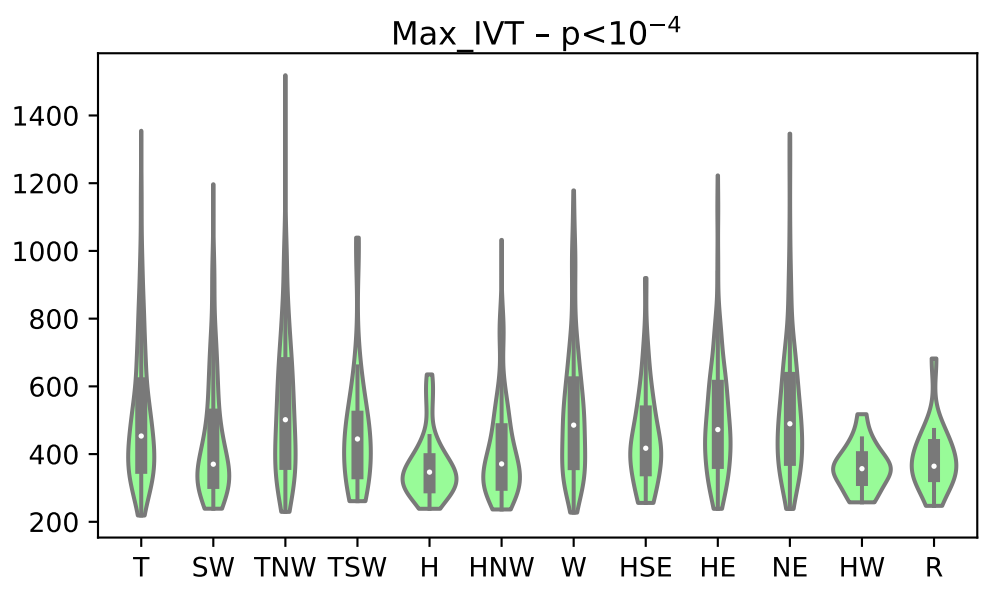
Max_IVT – p<10^{-4}
1400
1200
1000
800
600
400
200
T SW TNW TSW H HNW W HSE HE NE HW R

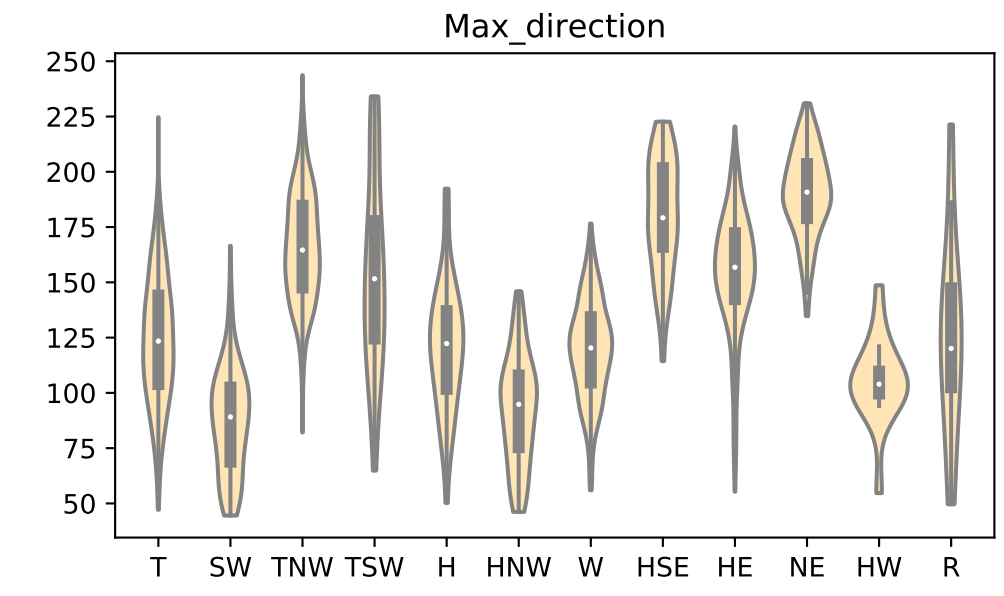
Max_direction
250
225
200
175
150
125
100
75
50
T SW TNW TSW H HNW W HSE HE NE HW R

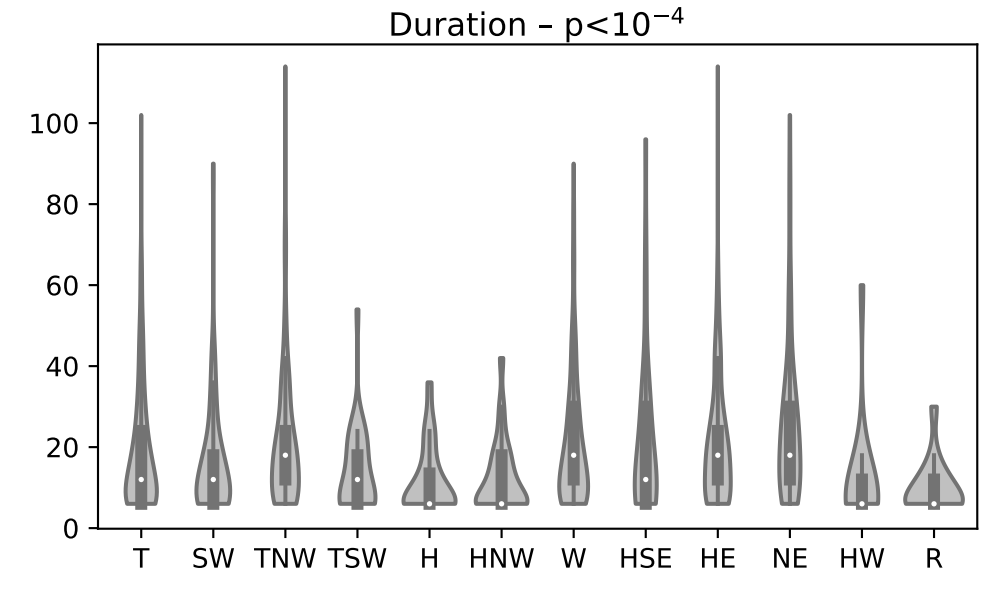
Duration – p<10^{-4}
100
80
60
40
20
0
T SW TNW TSW H HNW W HSE HE NE HW R

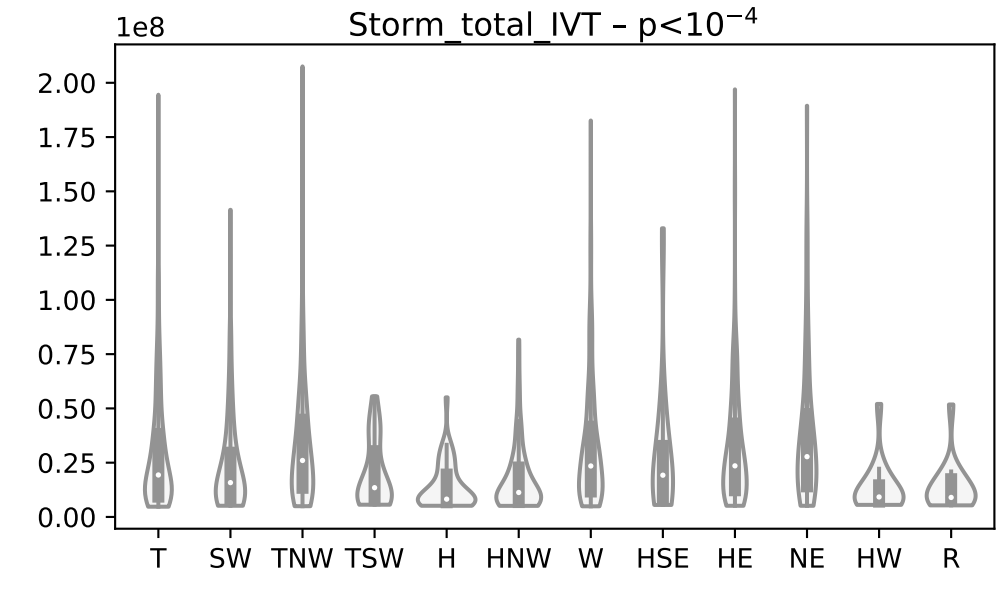
Storm_total_IVT – p<10^{-4}
1e8
2.00
1.75
1.50
1.25
1.00
0.75
0.50
0.25
0.00
T SW TNW TSW H HNW W HSE HE NE HW R

Figure 8a.

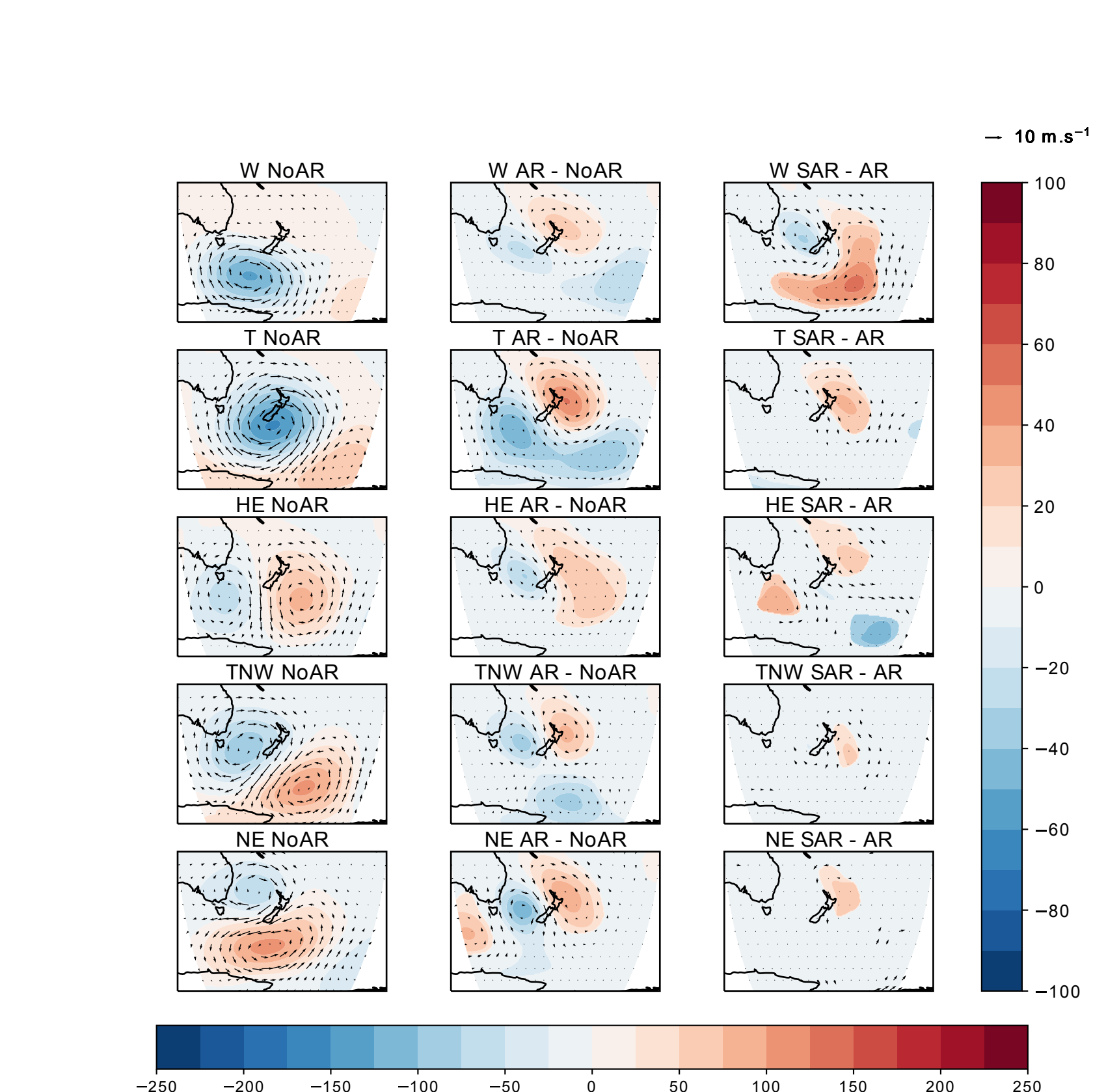
10 m.s−1
W NoAR
W AR - NoAR
W SAR - AR
T NoAR
T AR - NoAR
T SAR - AR
HE NoAR
HE AR - NoAR
HE SAR - AR
TNW NoAR
TNW AR - NoAR
TNW SAR - AR
NE NoAR
NE AR - NoAR
NE SAR - AR
100
80
60
40
20
0
−20
−40
−60
−80
−100
−250
−200
−150
−100
−50
0
50
100
150
200
250

Figure 8b.

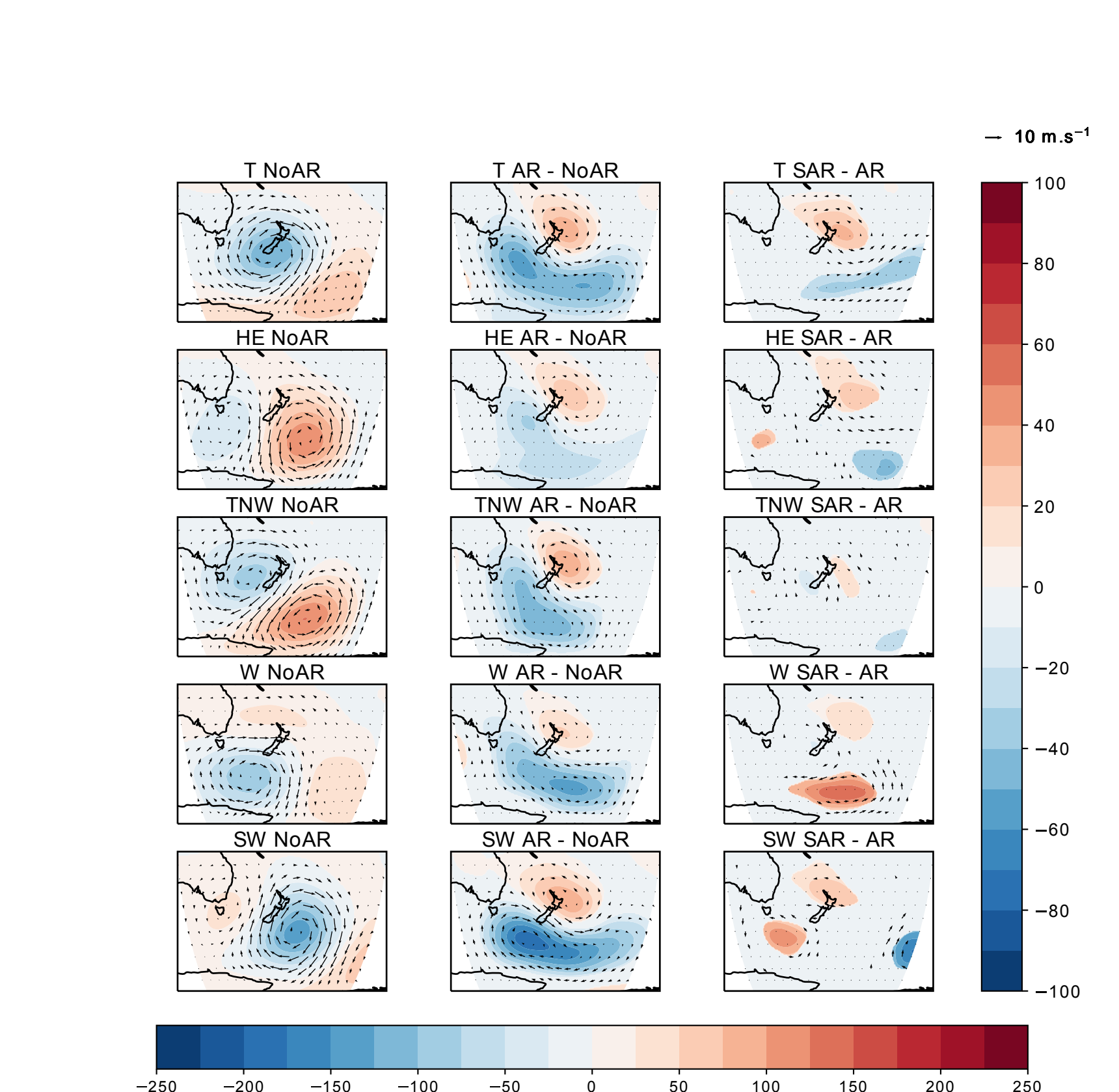
10 m.s−1
T NoAR
T AR - NoAR
T SAR - AR
HE NoAR
HE AR - NoAR
HE SAR - AR
TNW NoAR
TNW AR - NoAR
TNW SAR - AR
W NoAR
W AR - NoAR
W SAR - AR
SW NoAR
SW AR - NoAR
SW SAR - AR
100
80
60
40
20
0
−20
−40
−60
−80
−100
−250
−200
−150
−100
−50
0
50
100
150
200
250

Figure 9a.

W

	MinZ	LatMin	LonMin	MaxZ	LatMax	LonMax	DiffZ	DiffLat	DiffLon	Grad
AR_IVTx				**-0.18**			**-0.13**			
AR_IVTy	**-0.16**			**-0.18**	0.08			0.08		**-0.11**
AR_IVTmag	**0.11**						-0.09			0.09
Max_IVT				**-0.16**		-0.10	-0.11		**-0.12**	
Max_IVTx				**-0.21**		**-0.13**			**-0.12**	
Max_IVTy	**-0.12**									
Duration	-0.10			**-0.14**	**0.12**			0.10		
Storm_total_IVT				**-0.17**	0.10					

T

	MinZ	LatMin	LonMin	MaxZ	LatMax	LonMax	DiffZ	DiffLat	DiffLon	Grad
AR_IVTx		**-0.26**	**0.10**							
AR_IVTy	**-0.21**	**-0.21**	0.08							
AR_IVTmag										
Max_IVT										
Max_IVTx		**-0.29**								
Max_IVTy	**-0.20**	**-0.22**	**0.18**							
Duration	**-0.16**									
Storm_total_IVT										

HE

	MinZ	LatMin	LonMin	MaxZ	LatMax	LonMax	DiffZ	DiffLat	DiffLon	Grad
AR_IVTx	0.12			**-0.24**			**-0.25**			-0.11
AR_IVTy							-0.10			
AR_IVTmag										
Max_IVT				-0.13						
Max_IVTx				**-0.24**			**-0.20**			
Max_IVTy	0.11									
Duration	-0.13			-0.13	**0.18**					
Storm_total_IVT	-0.13			-0.13	**0.16**					

TNW

	MinZ	LatMin	LonMin	MaxZ	LatMax	LonMax	DiffZ	DiffLat	DiffLon	Grad
AR_IVTx		**-0.19**		**-0.22**			**-0.18**	0.10		
AR_IVTy		-0.10								
AR_IVTmag				-0.10						
Max_IVT				**-0.20**			-0.13			**-0.16**
Max_IVTx		**-0.19**		**-0.27**			**-0.20**	0.15		
Max_IVTy										0.14
Duration	**-0.16**			**-0.19**						
Storm_total_IVT				**-0.23**						-0.13

NE

	MinZ	LatMin	LonMin	MaxZ	LatMax	LonMax	DiffZ	DiffLat	DiffLon	Grad
AR_IVTx							-0.15		-0.15	**-0.19**
AR_IVTy										
AR_IVTmag										
Max_IVT			-0.20						0.22	
Max_IVTx										
Max_IVTy			0.21						-0.22	
Duration			-0.19						0.22	
Storm_total_IVT			-0.21						**0.22**	

Figure 9b.

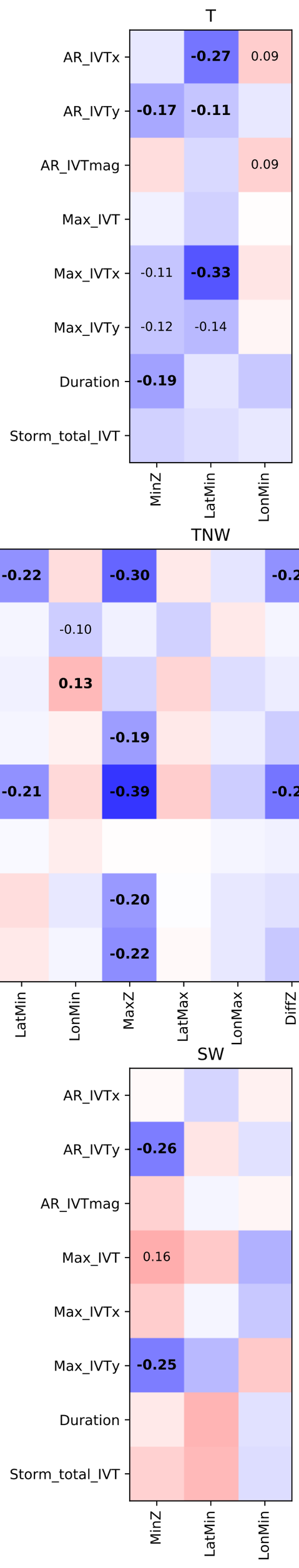
T
AR_IVTx -0.27 0.09
AR_IVTy -0.17 -0.11
AR_IVTmag 0.09
Max_IVT
Max_IVTx -0.11 -0.33
Max_IVTy -0.12 -0.14
Duration -0.19
Storm_total_IVT
MinZ LatMin LonMin
TNW
AR_IVTx -0.22 -0.30 -0.22 0.18
AR_IVTy -0.10
AR_IVTmag 0.13 -0.12
Max_IVT -0.19 -0.15
Max_IVTx -0.21 -0.39 -0.27 0.21
Max_IVTy
Duration -0.20 -0.15
Storm_total_IVT -0.22 -0.16
MinZ LatMin LonMin MaxZ LatMax LonMax DiffZ DiffLat DiffLon Grad
SW
AR_IVTx
AR_IVTy -0.26
AR_IVTmag
Max_IVT 0.16
Max_IVTx
Max_IVTy -0.25
Duration
Storm_total_IVT
MinZ LatMin LonMin

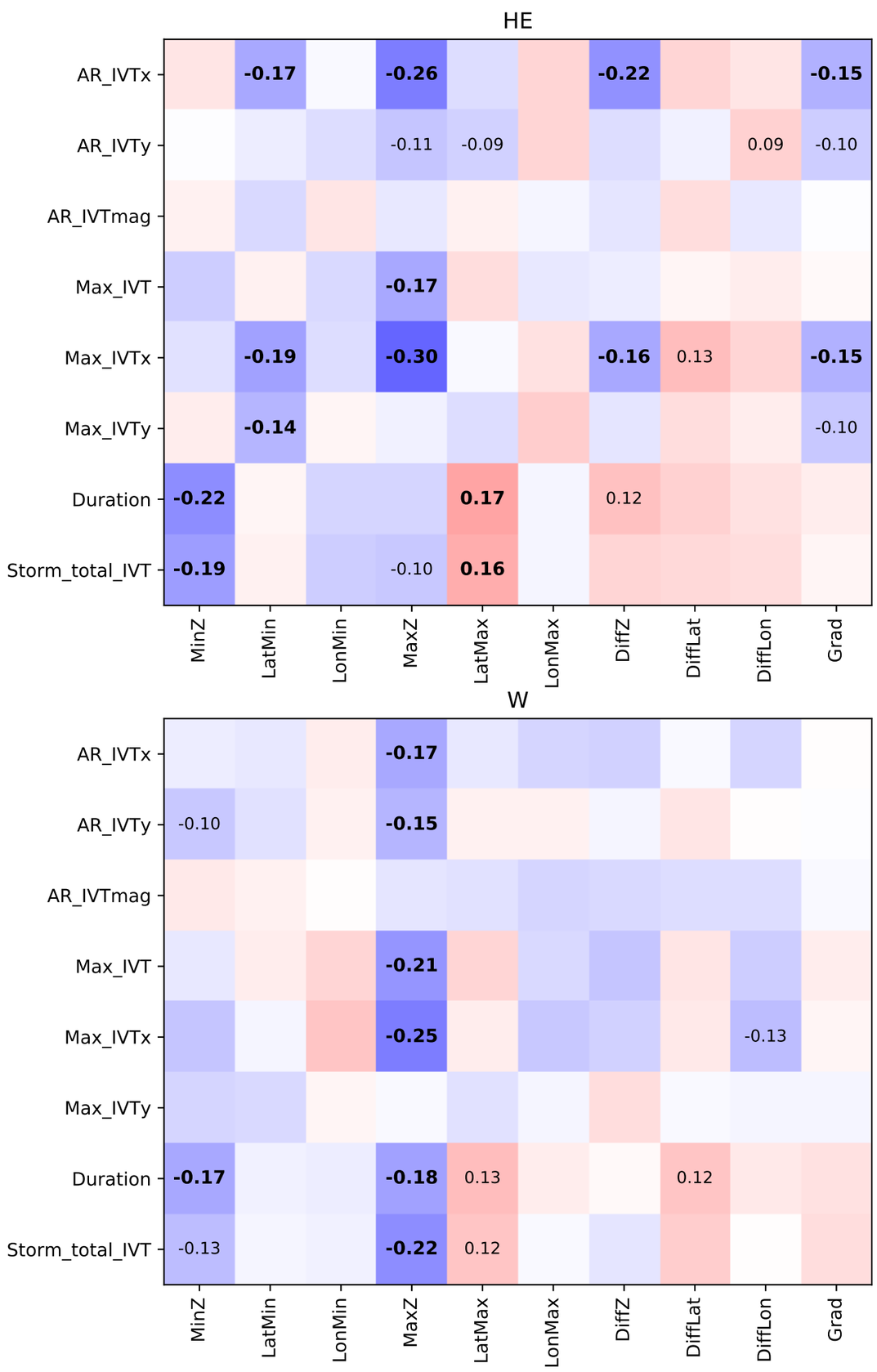
HE
AR_IVTx -0.17 -0.26 -0.22 -0.15
AR_IVTy -0.11 -0.09 0.09 -0.10
AR_IVTmag
Max_IVT -0.17
Max_IVTx -0.19 -0.30 -0.16 0.13 -0.15
Max_IVTy -0.14 -0.10
Duration -0.22 0.17 0.12
Storm_total_IVT -0.19 -0.10 0.16
MinZ LatMin LonMin MaxZ LatMax LonMax DiffZ DiffLat DiffLon Grad
W
AR_IVTx -0.17
AR_IVTy -0.10 -0.15
AR_IVTmag
Max_IVT -0.21
Max_IVTx -0.25 -0.13
Max_IVTy
Duration -0.17 -0.18 0.13 0.12
Storm_total_IVT -0.13 -0.22 0.12
MinZ LatMin LonMin MaxZ LatMax LonMax DiffZ DiffLat DiffLon Grad

Figure 10.

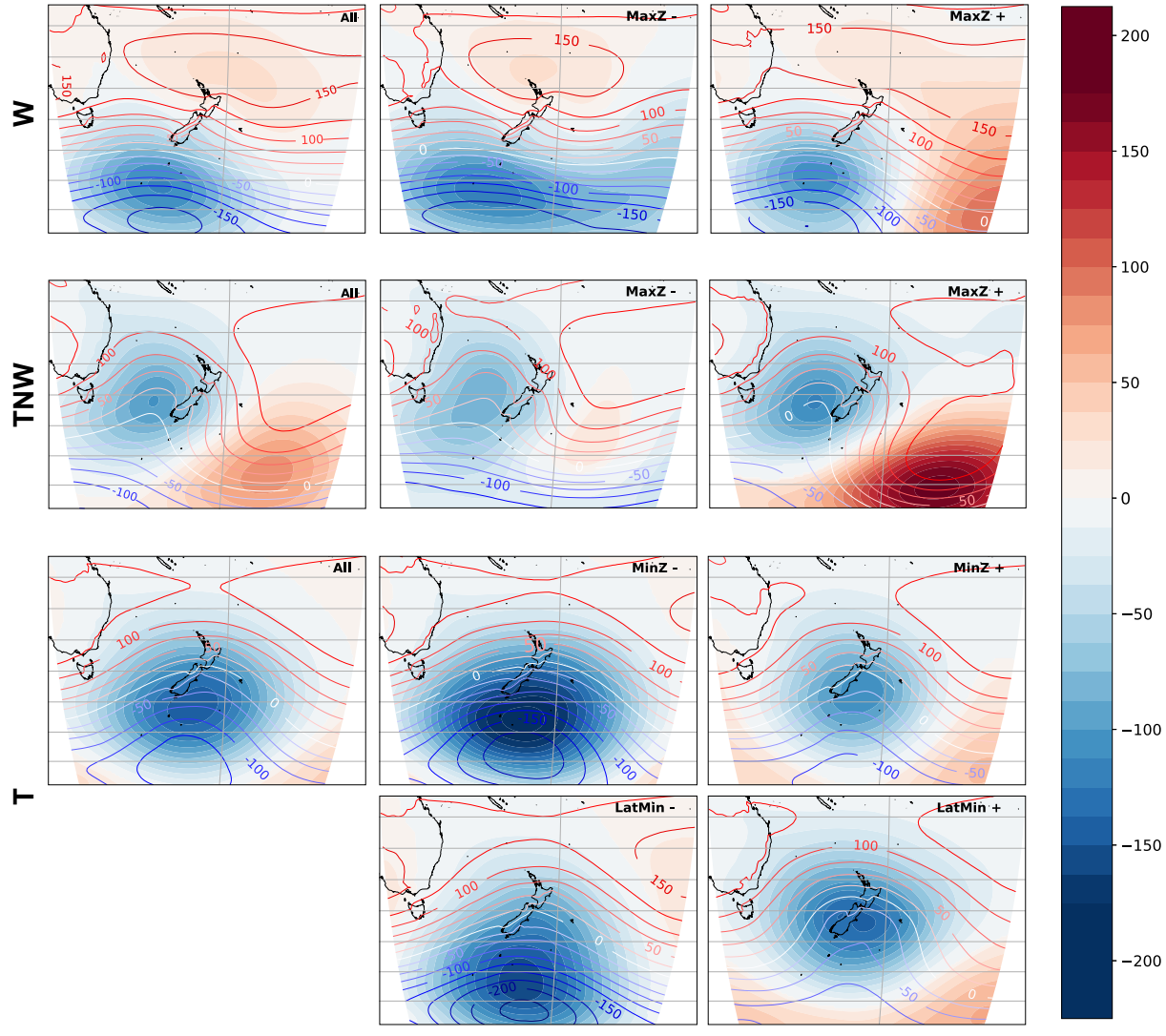
W
TNW
T
All
MaxZ -
MaxZ +
All
MaxZ -
MaxZ +
All
MinZ -
MinZ +
LatMin -
LatMin +
200
150
100
50
0
−50
−100
−150
−200